Title

Hox genes limit germ cell formation in the short germ insect *Gryllus bimaculatus*

Authors and Affiliations

Austen A. Barnett*[ac], Taro Nakamura*[bc], and Cassandra G. Extavour*[†]

* Department of Organismic and Evolutionary Biology, Harvard University, Cambridge MA, 02138.

[†] Department of Molecular and Cellular Biology, Harvard University, Cambridge MA, 02138.

[a] Current Address: Department of Natural Sciences, DeSales University, Center Valley, PA 18034

[b] Current Address: Division of Evolutionary Developmental Biology, National Institute for Basic Biology, 38, Nishigonaka, Myodaiji, Okazaki 444-8585, Japan

[c] Equal author contribution.

Correspondence

Cassandra G. Extavour extavour@oeb.harvard.edu

Keywords

Hox, *Gryllus bimaculatus*, insect, evo-devo, germ cells, *Sex-combs reduced, Antennapedia, Ultrabithorax, abdominal-A*.

Abstract

Hox genes are conserved transcription factor-encoding genes that specify the identity of body regions in bilaterally symmetrical animals. In the cricket *Gryllus bimaculatus*, a member of the hemimetabolous insect group Orthoptera, the induction of a subset of mesodermal cells to form the primordial germ cells (PGCs) is restricted to the second through the fourth abdominal segments (A2-A4). In numerous insect species, the Hox genes *Sex-combs reduced* (*Scr*), *Antennapedia* (*Antp*), *Ultrabithorax* (*Ubx*) and *abdominal-A* (*abd-A*) jointly regulate the identities of middle and posterior body segments, suggesting that these genes may restrict PGC formation to specific abdominal segments in *G. bimaculatus*. Here we show that all of these Hox genes, either individually or in segment-specific combinations, restrict PGC formation. Our data provides evidence for a segmental Hox code used to regulate the placement of PGC formation, reminiscent of the segmental Hox codes used in other arthropod groups to establish other aspects of segmental identity. These data also provide, to our knowledge, the first evidence for this ancient group of genes in determining PGC placement within the context of axial patterning in any animal studied thus far.

Introduction

The Hox genes are an ancient family of transcription factor-encoding genes that play a conserved role in specifying the body regions of bilaterally symmetrical animals during development (reviewed in 1). In arthropods, Hox genes act to specify the distinct identities of different body segments (reviewed in 2), with mutations in Hox genes usually resulting in switches of segmental type called homeotic transformations (reviewed in 3). We previously showed that in the cricket *Gryllus bimaculatus*, which belongs to the hemimetabolous insect order Orthoptera, the primordial germ cells (PGCs) form from the mesoderm of the second to the fourth abdominal segments (A2-A4) (4) via a bone morphogenetic protein (BMP)-dependent mechanism (5). Given that BMP activity is not limited to the segments where PGCs form, but rather, is present in the dorsal regions of all body segments (5), these data suggested that some unidentified factor or factors must ensure that PGCs form specifically in A2-A4. As Hox genes play a conserved role in establishing segmental identity, here we test the hypothesis that Hox genes contribute to regulating the placement of the PGCs in A2-A4.

Data implicating Hox genes in embryonic germ line placement in other animal taxa are scarce. In the mouse *Mus musculus*, as in *G. bimaculatus*, PGCs are established via BMP signals that activate the transcription factor Blimp-1 (5-7). Mouse embryonic cells that take on PGC fate repress the Hox genes *Hoxa1* and *Hoxb1* via activity of the BMP-activated transcription factor Blimp-1 (7-9). This has been interpreted as reflecting the loss of somatic differentiation programs that is associated with adopting PGC fate. Repression of Hox genes during differentiation of human induced pluripotent stem cells (hIPS) into in vitro derived PGCs (iPGCs) (10) is consistent with the hypothesis that Hox gene expression and PGC fate are mutually exclusive. In a system where germ cells are specified by inductive signals from neighboring cells, the degree or robustness of the PGC differentiation response may be influenced by the degree of concomitant Hox gene knockdown. Indeed, it was recently reported report that among mouse embryonic cells expressing PGC markers, there are some cells that also express hematopoietic markers, including at least one Hox gene (11). One interpretation of these observations is that those putative PGCs that respond to inductive signals by expressing lower levels of germ cell markers, may still be prone to express some somatic markers. Thus, it may be that decreased levels of somatic markers like Hox genes can facilitate the acquisition of PGC fate.

A role for HoxD genes in patterning and elongation of the external genitalia in mice has long been recognized (12-15), and HoxA genes are required for the correct development and function of elements of the female reproductive system that are derived from the Müllerian ducts, including the uterus and endometrium (16-19). However, the functions of Hox genes known to be expressed in the genital ridges, the precursors to the gonads (see for example 20), has received less attention. Taken together, these data suggest that there may be an important, but poorly studied, role for Hox genes in the context of PGC establishment and gonad positioning in animals with inductive PGC specification.

In contrast to *G. bimaculatus*, in the model insect *Drosophila melanogaster* PGCs form early in development (21, 22), long before the activation of the Hox genes that establish the identities of the body segments (23-26). Following gastrulation, the PGCs migrate towards the somatic gonad precursors (reviewed in 27), which develop from the mesoderm of embryonic abdominal parasegments 10-12 (28). The Hox genes *abdominal-A* (*abd-A*) and *Abdominal-B* (*Abd-B*) are necessary for the formation of the gonad precursors, which is independent of PGC specification. Specifically, *abd-A* establishes anterior gonad fates, and *abd-A* and *Abd-B* act in concert to establish the posterior gonad fates (28-31). In addition, in adult male *D. melanogaster*, *Abd-B* is required for correct function of the accessory gland (32), which is a component of the reproductive system that regulates the female response to mating (33). Moreover, this Hox gene is also required to maintain the identity of both germ line and somatic stem cells in the adult testis (34-37). However, these somatic and post-embryonic functions of *Abd-B* do not affect embryonic PGC establishment in *D. melanogaster*, which takes places much earlier in development.

Across insects, the Hox genes *Sex-combs reduced (Scr)*, *Antennapedia (Antp), Ultrabithorax (Ubx)* and *abdominal-A (abd-A)* have a conserved role in establishing the thoracic and abdominal segments during embryogenesis (reviewed in 2). To explore the role of these Hox genes in establishing *G. bimaculatus* PGCs, we used embryonic RNAi (eRNAi) to repress the function of each of these genes individually, and also in combination. We found that these Hox genes act within the abdomen in a segment-specific manner to restrict PGC formation. Reminiscent of their combinatorial action in specifying other aspects of segment identity, including ectodermal patterning and appendage differentiation, these data suggest that a “Hox code” is also needed for appropriate PGC specification. These are the first data, to our knowledge, demonstrating a role for these highly conserved and ancient genes in limiting germ line

development in an animal, and provide evidence for an additional embryonic role of Hox genes outside of establishing anterior-posterior segmental identity.

Results and Discussion

G. bimaculatus PGCs emerge from the lateral mesoderm of abdominal segments A2-A4, within the mesoderm of each hemisegment (*i.e.*, the left or right halves of the segment) bearing the PGCs (4). Four Hox genes, *Scr* (*Gb-Scr*), *Antp* (*Gb-Antp*), *Ubx* (*Gb-Ubx*) and *abd-A* (*Gb-abd-A*) (Figs. S1, S2), are expressed in the abdomen during *G. bimaculatus* embryogenesis (38, 39). To investigate whether these posterior Hox genes were expressed at a time and place that would enable them to supply segment-specific positional information for PGC development, we performed *in situ* hybridization during PGC formation. As previously described (38, 39), these Hox genes exhibit spatial collinearity in the ectoderm from gnathal to abdominal segments in wild type embryos at stage 8, a stage when all segments have been defined and are morphologically distinct (Fig. 1 and Fig. S*3*). Because PGCs arise from the abdominal mesoderm, we asked whether these Hox genes were also expressed in the mesoderm. *Gb-Scr*, *Gb-Antp* and *Gb-abd-A* transcripts were expressed in the mesodermal cells of the abdominal segments (Fig. 1B, C, E), whereas *Gb-Ubx* transcripts were not detected above background levels in the dorsal mesodermal cells of A2-A10, but rather appeared to be restricted to the ectoderm in these segments (Fig. 1D).

To determine whether the mesodermally-expressed Hox genes were also expressed in PGCs, we conducted co-detection of Piwi protein, a PGC marker in *G. bimaculatus* (4), and Hox gene transcripts. We detected *Gb-Scr, Gb-Antp* and *Gb-abd-A* transcripts in mesodermal cells adjacent to PGCs at stages 7-8.5, but transcripts were undetectable or at very low levels in the PGCs themselves (Fig. 1B). Gb-Ubx expression was also undetectable in the PGCs at these stages (Fig. 1D, I). Taken together, these results suggest that, as in mice, *G. bimaculatus* Hox gene transcription is active in somatic cells adjacent to PGCs, but is repressed or inactive within PGCs (7-9).

Given their expression in cells in close proximity to PGCs, we hypothesized that these Hox genes might play a role in PGC formation, placement, or maintenance. To test this hypothesis, we used embryonic RNA interference (eRNAi) to abrogate the activity of one or more of these Hox genes during

G. bimaculatus embryogenesis (Table S1), and assessed the effect on PGC number and segmental position. Specifically, we compared the PGC number per hemisegment and per embryo, as well as the presence or absence of PGC clusters in each hemisegment, to controls (Supplementary Materials and Methods; Tables S2-S7).

eRNAi against *Gb-Scr* efficiently depleted *Gb-Scr* transcripts as assessed by qPCR (Fig. *S4*), although this was not accompanied by transformation of gnathal appendages to a thoracic identity (n=36; Fig. 2L), as is often observed upon *Scr* knockdown in other insects (e.g. 40, 41). *Gb-Scr* eRNAi did, however, result in an increase in PGC number as well as a significant number of segments bearing PGC clusters in A2-A4 relative to controls (Fig. 2*A-B, F-G*). Furthermore, the total number of PGCs per embryo increased significantly relative to control injections (Fig. 2*K*).

eRNAi against *Gb-Antp*, similarly to the *Gb-Scr* eRNAi treatment, did not result in a homeotic phenotype (n=14; Fig. 2L). However, our qPCR results showed that this treatment was also sufficient to reduce *Gb-Antp* transcripts (Fig. *S4*). *Gb-Antp* eRNAi significantly increased the proportion of segments bearing PGC clusters in A1-A4, and also increased PGC number in A2 (Figs. 2*C, H*) and overall (Fig. 2*K*). Thus, loss of *Gb-Antp* resulted both in additional PGCs in the correct segments, as did loss of *Gb-Scr*, and also in ectopic PGCs in A1.

Gb-Ubx eRNAi resulted in the transformation of A1 appendages (pleuropodia) towards ectopic walking legs (n=28/41; Figs. 2L, *SB5, S6B, F, S7A*), supported by expression of the appendage marker *Distal-less* (*Dll*) (42) (Fig. S6B) and reduced expression of the *G. bimaculatus* orthologue of *tramtrack* (*ttk*), a gene that shows enriched expression in pleuropodia (Fig. S6F), and consistent with *Ubx* knockdowns in other insects (43-46). Furthermore, qPCR showed that dsRNA injections reduced *Gb-Ubx* transcripts (Fig. *S4*). However, *Gb-Ubx* eRNAi did not significantly affect PGC number, or the numbers of PGC clusters, in any segment, or overall, relative to controls (Figs. 2*D, I* and *K*).

eRNAi targeting *Gb-abd-A* transcripts resulted in ectopic appendages throughout all abdominal segments (n=19/25; Figs. 2L, S*5C, S6C, G, S7B*). These ectopic outgrowths expressed *Dll* (Fig. S6C) but not *ttk* (Fig. S6G), and were consistent with outgrowths observed in *abd-A* knockdowns in other insects (43, 47-50). qPCR confirmed a decrease in *Gb-abd-A* transcripts following the eRNAi treatment (Fig. *S4*). *Gb-abd-A* eRNAi increased both PGC number in A2, and also the proportion of hemisegments bearing

PGC clusters in A3 (Figs. 2*E*, *J* and *K*). Together, the results of these single Hox gene knockdowns suggest that *Gb-Scr* and *Gb-abd-A* represses mesodermal transformation to PGCs in A2-A3, and that *Gb-Antp* represses PGC formation in A1-A4.

In arthropods, Hox genes often work in concert to either activate or repress transcriptional targets (reviewed in 2). Therefore, we explored the possibility that the aforementioned Hox genes could be acting together in the context of PGC specification. We predicted that if a combination of Hox genes worked together to modulate PGC formation, a double knockdown of these genes would result in unique PGC defects relative to the defects observed in the single knockdowns discussed above. To test this prediction, we systematically injected embryos with equal amounts of dsRNA targeting each pairwise combination of these posterior *G. bimaculatus* Hox genes (Table *S1*).

Unexpectedly, all double eRNAi treatments that involved *Gb-Scr* dsRNA as a partner resulted in embryonic lethality one day after injection (Table *S1*). We therefore could not study its interaction with the other Hox genes eRNAi simultaneously targeting *Gb-Antp* and *Gb-Ubx* resulted in the same embryonic homeotic transformation as *Gb-Ubx* single knockdowns (*i.e.*, an ectopic fourth leg on A1, n=27/31; Fig. *S5D, S7C*). This double knockdown also resulted an increase in the presence of PGCs in A2-A5, as well as an increase in the number of PGCs in segments A2-A4 and overall compared to controls (Figs *3A*, *D, E*). Comparing these results to the *Gb-Ubx* and *Gb-Antp* single knock-downs, the overall PGC increase induced by the double knockdown (Fig. 3D) was not significantly different than that induced by *Gb-Antp* knockdown alone (Fig. 2K), suggesting that *Gb-Antp* act alone to repress PGC formation in A2-A4. However, the reduction in A1 PGC number in the double knockdown (Fig. 3A) relative to *Gb-Antp* alone (Fig. 2H), suggests that *Gb-Antp* acts to repress a PGC formation-promoting function of *Gb-Ubx* in A1. Furthermore, the presence of significantly more PGC clusters in A5 in the double knockdown (Fig. 3A, E) relative to both single knockdowns (Fig. 2H, I) also suggests that these genes act together to repress PGC formation in A5.

RNAi simultaneously targeting *Gb-Ubx* and *Gb-abd-A* resulted in embryos with ectopic legs throughout the abdomen (n=8/14; Fig. *S5E, S7D*), exhibiting a similar phenotype to other studied insects (43, 49). These embryos also have significantly more PGC clusters in A3 and A4 compared to controls, as well as an increase in total PGC number in A4 (Figs. 3*B, F*). However, the overall increase in PGCs

per embryo compared to controls was not statistically significant (Table S3). Comparing these results to the *Gb-Ubx* and *Gb-abd-A* single knockdowns suggests that *Gb-abd-A* alone is restricting PGC formation in A3, and that both *Gb-Ubx* and *Gb-abd-A* act together to restrict PGC formation in A4 (compare Fig. 2I, J with Fig 3*B*).

RNAi of *Gb-Antp* and *Gb-abd-A* together did not result in any detectable embryonic homeotic phenotype (data not shown). However, the effect on PGC formation in these embryos was striking: A1-A6 contained significantly more PGC clusters in A1-6 than controls (Figs. 3*C*, *D,* and *G*), and there were significantly more PGCs in A2-A4, and overall. Comparing this double knockdown to the single *Gb-Antp* and *Gb-abd-A* knockdowns revealed that the PGC increase caused by *Gb-Antp* eRNAi alone (Fig. 2H) was slightly suppressed in A2 (Fig. 3C), revealing a potential role of *Gb-Antp* in repressing *Gb-abd-A's* ability to promote PGC formation in A2. Furthermore, this double knockdown provided evidence that *Gb-Antp* and *Gb-abd-A* act together to suppress PGC development in A3-A4, A6 and overall (Fig. *3D* and *G*).

Together, our results provide evidence for a Hox "code" specific to the formation of PGCs in *G. bimaculatus* abdominal segments (Fig. 4). We also propose that this "code" is at least partially separate from that encoding segmental identity, as the resulting Hox embryonic homeotic phenotypes do not always correlate with PGC positioning defects. For example, when we repress *Gb-abd-A* via eRNAi, A2-A3 bear pleuropodia-like appendages (Figs. *S5, S6*). In wild-type embryos, the pleuropodia are on A1, and thus we might expect that in this eRNAi condition, A2-A3 are transformed to an A1 identity. As the A1 segment generally lacks PGCs (4, 5), we should not observe PGCs in these segments in *Gb-abd-A* eRNAi injected embryos. However, we see an increase in PGCs in these segments in this condition (Fig. 2J). In another example, *Gb-Ubx*+*Gb-abd-A* eRNAi embryos bear ectopic leg-like structures on all abdominal segments (Fig. S5E). Being that *G. bimaculatus* wild-type embryos lack PGCs on their leg-bearing (thoracic) segments (4), we might expect an absence of Hox genes in A2-A4 in this eRNAi condition. However, we instead see an increase in the presence of PGCs in these segments (Fig. 3B).

Hox codes that are used to pattern organs outside of the primary antero-posterior axes of animals have been described in other animal taxa. Examples include the use of Hox genes to pattern the proximo-distal axes of the tetrapod autopod (reviewed in 51), the branchial region of the vertebrate head (52), and the vertebrate neural tube (53). In insects, such non-axial Hox roles have also been previously described,

such as those needed for the positioning of the bacteriomes in the seed bug *Nysius plebeius* (48), the formation of the lantern organ in the firefly *Photuris (sp.)* (54), and the differentiation of a specific accessory gland cell type in male fruit flies (32). Our results provide an example of Hox genes being used to coordinate cell type specification (PGCs) to ensure correct organ (gonad) positioning in the context of the body plan.

Our results suggest that Hox genes may play an indirect role in PGC specification. As has been suggested in the case of mouse PGC specification (7, 8, 55), downregulation of Hox genes may suppress somatic fate, permitting or facilitating adoption of PGC fate by BMP-responding cells. Alternatively, Hox genes may act in the somatic cells adjacent to PGCs to negatively regulate PGC fate, thus restricting the number of cells that can adopt PGC fate, or limiting the position where PGCs emerge in the abdominal segments.

The Hox code needed for the development of *G. bimaculatus* PGCs in A2-A4 may act to position these PGCs in an area where the gonad must form. *G. bimaculatus* PGCs do not undergo long-range migration (5), and the cells of the somatic gonad primordia are thought to lie within A2-A4 (4). To explore this possibility, we asked if *G. bimaculatus* orthologues of *Six4* and *eyes absent* (*eya*), gonad primordia markers used in *Drosophila* (56, 57), could identify putative somatic gonad precursors in *G. bimaculatus*. However, *in situ* hybridization did not show enhanced expression of either gene in cells adjacent to PGCs in A2-A4 (Fig. *S8*). These data suggest that either the gonad primordia are specified at later stages, or that these genes are not used to specify gonad primordia in *G. bimaculatus*. Further work will thus be needed to determine whether the increase in PGCs induced by many of the Hox eRNAi conditions is at the expense of mesoderm that would have been fated to be somatic gonadal cells in wild type embryos.

As in other animals with discrete gonads, arthropod PGCs must meet with somatic gonad cells and end up in a specific location in the body to form a functional gonad. In arthropods, the location of the gonad and often the location of PGCs when they first arise, is tied to specific body segments. In insects like *Drosophila*, where PGCs form much earlier than Hox gene activation and must migrate to the primordial gonad, the somatic gonad precursors rely on Hox genes to form in specific segments (28). In the beetle *Tenebrio molitor*, distinct PGC clusters form in many abdominal segments, and then coalesce into those segments that will ultimately contain the gonads (58). In the firebrat *Thermobia domestica* and

the stick insect *Carausius morosus*, PGCs are thought to originate as a long cluster spanning multiple segments, before ultimately becoming confined to the gonads within specific segments (reviewed in59). Outside of insects, in the spider *Parasteatoda tepidariorum*, the germ cells also arise as clusters, which are situated in the opisthosomal segments 2-6 (60). Taken together with the functional genetic data presented here, we suggest that assigning the PGC-bearing segments may be an ancestral role for Hox genes in arthropods.

Materials and Methods

All Hox genes were cloned using a previously published *G. bimaculatus* transcriptome (61). The predicted translations of the resulting sequences were subjected to phylogenetic analysis to corroborate orthology (Fig. *S2*). Animal husbandry, eRNAi (Table S1), embryonic staging, cloning and qPCR (Table S8), *in situ* hybridizations and immunostainings, statistical tests and PGC quantifications were performed as previously described (4-6, 62). See Supplementary Material for detailed methods.

Acknowledgments

We thank Dr. Taro Mito (University of Tokushima) for kindly allowing us access to draft genomic data for *G. bimaculatus*. This work was supported by NSF award IOS-1257217 to CGE.

References

1. Hrycaj SM & Wellik DM (2016) Hox genes and evoution. *F1000Res* 5:859.
2. Hughes CL & Kaufman TC (2002) Hox genes and the evolution of the arthropod body plan. *Evol. Dev.* 4(6):459-499.
3. Hombria JCG & Lovegrove B (2003) Beyond homeosis - HOX function in morphogenesis and organogenesis. *Differentiation* 71(8):461-476.
4. Ewen-Campen B, Donoughe S, Clarke DN, & Extavour CG (2013) Germ cell specification requires zygotic mechanisms rather than germ plasm in a basally branching insect. *Curr. Biol.* 23(10):835-842.
5. Donoughe S*, et al.* (2014) BMP signaling is required for the generation of primordial germ cells in an insect. *Proc. Natl. Acad. Sci. USA* 111(11):4133-4138.
6. Nakamura T & Extavour CG (2016) The transcriptional repressor Blimp-1 acts downstream of BMP signaling to generate primordial germ cells in the cricket *Gryllus bimaculatus*. *Development* 143(2):255-263.
7. Ohinata Y*, et al.* (2005) Blimp1 is a critical determinant of the germ cell lineage in mice. *Nature* 436(7048):207-213.
8. Saitou M, Barton SC, & Surani MA (2002) A molecular programme for the specification of germ cell fate in mice. *Nature* 418(6895):293-300.
9. Kurimoto K*, et al.* (2008) Complex genome-wide transcription dynamics orchestrated by Blimp1 for the specification of the germ cell lineage in mice. *Genes Dev.* 22(12):1617-1635.
10. Park TS*, et al.* (2009) Derivation of primordial germ cells from human embryonic and induced pluripotent stem cells is significantly improved by coculture with human fetal gonadal cells. *Stem Cells* 27(4):783-795.
11. Scaldaferri ML*, et al.* (2015) Hematopoietic activity in putative mouse primordial germ cell populations. *Mech. Dev.* 136:53-63.
12. Dolle P & Duboule D (1989) Two gene members of the murine HOX-5 complex show regional and cell-type specific expression in developing limbs and gonads. *EMBO J.* 8(5):1507-1515.
13. Zakany J, Fromental-Ramain C, Warot X, & Duboule D (1997) Regulation of number and size of digits by posterior Hox genes: a dose-dependent mechanism with potential evolutionary implications. *Proc. Natl. Acad. Sci. USA* 94(25):13695-13700.
14. Cobb J & Duboule D (2005) Comparative analysis of genes downstream of the Hoxd cluster in developing digits and external genitalia. *Development* 132(13):3055-3067.
15. Dollé P, Brown J-CI-BM, Tickle C, & Duboule D (1991) Hox-4 genes and the morphogenesis of mammalian genitalia. *Genes Dev.* 5(10):1767-1776.
16. Du H & Taylor HS (2015) The Role of Hox Genes in Female Reproductive Tract Development, Adult Function, and Fertility. *Cold Spring Harb Perspect Med* 6(1):a023002.
17. Xu B*, et al.* (2014) Regulation of endometrial receptivity by the highly expressed HOXA9, HOXA11 and HOXD10 HOX-class homeobox genes. *Hum. Reprod.* 29(4):781-790.
18. Ma Y*, et al.* (2012) Knockdown of Hoxa11 in vivo in the uterosacral ligament and uterus of mice results in altered collagen and matrix metalloproteinase activity. *Biol. Reprod.* 86(4):100.
19. Ekici AB*, et al.* (2013) HOXA10 and HOXA13 sequence variations in human female genital malformations including congenital absence of the uterus and vagina. *Gene* 518(2):267-272.
20. Gaunt SJ, Coletta PL, Pravtcheva D, & Sharpe PT (1990) Mouse Hox-3.4: homeobox sequence and embryonic expression patterns compared with other members of the Hox gene network. *Development* 109(2):329-339.
21. Huettner AF (1923) The origin of the germ cells in *Drosophila melanogaster*. *J. Morphol.* 2(37):385-422.
22. Lehmann R (2016) Germ Plasm Biogenesis--An Oskar-Centric Perspective. *Curr. Top. Dev. Biol.* 116:679-707.
23. Akam M & Martinez-Arias A (1985) The distribution of *Ultrabithorax* transcripts in *Drosophila* embryos. *EMBO Journal* 4(7):1689-1700.
24. Levine M, Hafen E, Garber RL, & Gehring WJ (1983) Spatial distribution of Antennapedia transcripts during Drosophila development. *EMBO J.* 2(11):2037-2046.
25. Martinez-Arias A (1986) The Antennapedia gene is required and expressed in parasegments 4 and 5 of the Drosophila embryo. *EMBO J.* 5(1):135-141.

26. Martinez-Arias A, Ingham PW, Scott MP, & Akam ME (1987) The spatial and temporal deployment of Dfd and Scr transcripts throughout development of Drosophila. *Development* 100(4):673-683.
27. Santos AC & Lehmann R (2004) Germ Cell Specification and Migration in Drosophila and beyond. *Curr Biol* 14(14):R578-R589.
28. Boyle M & DiNardo S (1995) Specification, migration and assembly of the somatic cells of the *Drosophila* gonad. *Development* 121(6):1815-1825.
29. Greig S & Akam M (1995) The role of homeotic genes in the specification of the *Drosophila* gonad. *Curr. Biol.* 9(5):1057-1062.
30. Moore LA, Broihier HT, Van Doren M, Lunsford LB, & Lehmann R (1998) Identification of genes controlling germ cell migration and emryonic gonad formation in *Drosophila*. *Development* 125(4):667-678.
31. Riechmann V, Rehorn KP, Reuter R, & Leptin M (1998) The genetic control of the distinction between fat body and gonadal mesoderm in *Drosophila*. *Development* 125(4):713-723.
32. Gligorov D, Sitnik JL, Maeda RK, Wolfner MF, & Karch F (2013) A novel function for the Hox gene Abd-B in the male accessory gland regulates the long-term female post-mating response in Drosophila. *PLoS Genet* 9(3):e1003395.
33. Leopold RA (1976) The role of male accessory glands in insect reproduction. *Annual Review of Entomology* 21:199-221.
34. Zhang S*, et al.* (2017) Repression of Abd-B by Polycomb is critical for cell identity maintenance in adult Drosophila testis. *Sci Rep* 7(1):5101.
35. Morillo Prado JR, Chen X, & Fuller MT (2012) Polycomb group genes Psc and Su(z)2 maintain somatic stem cell identity and activity in Drosophila. *PLoS ONE* 7(12):e52892.
36. Papagiannouli F, Schardt L, Grajcarek J, Ha N, & Lohmann I (2014) The Hox gene Abd-B controls stem cell niche function in the Drosophila testis. *Dev Cell* 28(2):189-202.
37. Schardt L, Ander JJ, Lohmann I, & Papagiannouli F (2015) Stage-specific control of niche positioning and integrity in the Drosophila testis. *Mech. Dev.* 138(3):336-348.
38. Zhang H*, et al.* (2005) Expression patterns of the homeotic genes *Scr*, *Antp*, *Ubx*, and *abd-A* during embryogenesis of the cricket *Gryllus bimaculatus*. *Gene Expr Patterns* 5(4):491-502.
39. Matsuoka Y*, et al.* (2015) Short germ insects utilize both the ancestral and derived mode of Polycomb group-mediated epigenetic silencing of Hox genes. *Biol Open* 4(6):702-709.
40. Hughes CL & Kaufman TC (2000) RNAi analysis of *Deformed*, *proboscipedia* and *Sex combs reduced* in the milkweed bug *Oncopeltus fasciatus*: novel roles for Hox genes in the hemipteran head. *Development* 127(17):3683-3694.
41. Hrycaj S, Chesebro J, & Popadic A (2010) Functional analysis of Scr during embryonic and post-embryonic development in the cockroach, Periplaneta americana. *Dev. Biol.* 341(1):324-334.
42. Panganiban G*, et al.* (1997) The origin and evolution of animal appendages. *PNAS* (94):5162-5166.
43. Angelini DR, Liu PZ, Hughes CL, & Kaufman TC (2005) Hox gene function and interaction in the milkweed bug Oncopeltus fasciatus (Hemiptera). *Dev. Biol.* 287(2):440-455.
44. Bennett RL, Brown SJ, & Denell RE (1999) Molecular and genetic analysis of the *Tribolium Ultrabithorax* ortholog, *Ultrathorax*. *Dev. Genes Evol.* 209(10):608-619.
45. Zheng Z, Khoo A, Fambrough D, Garza L, & Booker R (1999) Homeotic gene expression in the wild-type and a homeotic mutant of the moth *Manduca sexta*. *Dev. Genes Evol.* 209(8):460-472.
46. Khila A, Abouheif E, & Rowe L (2009) Evolution of a novel appendage ground plan in water striders is driven by changes in the Hox gene Ultrabithorax. *PLoS Genet* 5(7):e1000583.
47. Sánchez-Herrero E, Guerrero I, Sampedro J, & González-Reyes A (1994) Developmental consequences of unrestricted expression of the *abd-A* gene of *Drosophila*. *MOD* 46(3):153-167.
48. Matsuura Y, Kikuchi Y, Miura T, & Fukatsu T (2015) Ultrabithorax is essential for bacteriocyte development. *Proc Natl Acad Sci U S A* 112(30):9376-9381.
49. Lewis DL, DeCamillis M, & Bennett RL (2000) Distinct roles of the homeotic genes *Ubx* and *abd-A* in beetle embryonic abdominal appendage development. *Proceedings- National Academy of Sciences USA* 97(9):4504-4509.
50. Stuart JJ, Brown SJ, Beeman RW, & Denell RE (1993) The Tribolium homeotic gene Abdominal is homologous to abdominal-A of the Drosophila bithorax complex. *Development* 117(1):233-243.

51. Leite-Castro J, Beviano V, Rodrigues PN, & Freitas R (2016) HoxA Genes and the Fin-to-Limb Transition in Vertebrates. *Journal of Developmental Biology* 4(1):10.
52. Hunt P*, et al.* (1991) A distinct Hox code for the branchial region of the vertebrate head. *Nature* 353(6347):861-864.
53. Hunt P & Krumlauf R (1992) Hox codes and positional specification in vertebrate embryonic axes. *Annu. Rev. Cell Biol.* 8:227-256.
54. Stansbury MS & Moczek AP (2014) The function of Hox and appendage-patterning genes in the development of an evolutionary novelty, the Photuris firefly lantern. *Proc Biol Sci* 281(1782):20133333.
55. Kurimoto K, Yamaji M, Seki Y, & Saitou M (2008) Specification of the germ cell lineage in mice: a process orchestrated by the PR-domain proteins, Blimp1 and Prdm14. *Cell Cycle* 7(22):3514-3518.
56. Clark IB, Jarman AP, & Finnegan DJ (2007) Live imaging of *Drosophila* gonad formation reveals roles for *Six4* in regulating germline and somatic cell migration. *BMC Developmental Biology* 7:52.
57. Boyle M, Bonini N, & DiNardo S (1997) Expression and function of *clift* in the development of somatic gonadal precursors within the *Drosophila* mesoderm. *Development* 5(124):971-982.
58. Ullmann SL (1964) The origin and structure of the mesoderm and the formation of the coelomic sacs in *Tenebrio molitor* L. (Insecta, Coleoptera). *Philos. Trans. R. Soc. Lond. B. Biol. Sci.* 248(747):245-277.
59. Koch M, Quast B, & Bartolomaeus T (2014) Coeloms and nephridia in annelids and arthropods. *Deep Metazoan Phylogeny: The Backbone of the Tree of Life*, eds Wägele JW & Bartolomaeus T (De Gruyter, Berlin), pp 173-284.
60. Schwager EE, Meng Y, & Extavour CG (2015) *vasa* and *piwi* are required for mitotic integrity in early embryogenesis in the spider *Parasteatoda tepidariorum*. *Dev. Biol.* 402(2):276-290
61. Zeng V*, et al.* (2013) Developmental gene discovery in a hemimetabolous insect: *de novo* assembly and annotation of a transcriptome for the cricket *Gryllus bimaculatus*. *PLoS ONE* 8(5):e61479.
62. Donoughe S & Extavour CG (2016) Embryonic development of the cricket *Gryllus bimaculatus*. *Dev. Biol.* 411(1):140-156.
63. Edgar RC (2004) MUSCLE: a multiple sequence alignment method with reduced time and space complexity. *BMC Bioinformatics* 5:113.
64. Lefort V, Longueville JE, & Gascuel O (2017) SMS: Smart Model Selection in PhyML. *Mol. Biol. Evol.* 34(9):2422-2424.
65. Guindon S & Gascuel O (2003) A simple, fast, and accurate algorithm to estimate large phylogenies by maximum likelihood. *Syst. Biol.* 52(5):696-704.

Figure Legends

Fig. 1. Posterior Hox gene expression adjacent to but absent from *G. bimaculatus* PGCs. (A,F) Schematic illustration of the embryonic stages (St.) (62) used for expression analysis. Red rectangle shows enlarged area in B-E and G-J'. *In situ* hybridization for *Gb-Scr*, *Gb-Antp*, *Gb-Ubx* and *Gb-abd-A* expression in the third abdominal segment (A3) at ES 7 (B-E) and ES 8.5 (G-J) of wild type embryos. (B'-J') Co-staining with Gb-Piwi protein in A3. (B,G) Expression of *Gb-Scr* is enriched in the abdominal mesoderm and undetectable above background levels in the ectoderm. (B',G') Co-staining with Gb-Piwi protein reveals *Gb-Scr* expression is excluded from PGCs. (C,H) *Gb-Antp* expression is detected in abdominal mesoderm and ectoderm. (C',H') *Gb-Antp* transcript is undetectable in *G. bimaculatus* PGCs at St. 7 and at very low levels at St. 8.5. (D,I) Weak *Gb-Ubx* expression is observed in the ventral mesoderm of A3. (D',I') PGCs do not detectably express *Gb-Ubx*. (E,J) High *Gb-abd-A* expression is detected in the A3 ectoderm and mesoderm. (E',J') PGCs display lower expression levels of *Gb-abd-A* than the adjacent mesoderm. Scale bars = 100 μm in B (applies to B-E'), G (applies to G-J').

Fig. 2. Embryonic RNA interference (eRNAi) of *Gb-Scr*, *Gb-Antp* and *Gb-abd-A* increases in PGC number. (*A-E*) Confocal images of the A2-A5 of a representative embryo from each knockdown condition as well as the control condition (*DsRed* eRNAi). Gb-Piwi (magenta) marks PGC clusters (arrowheads) (4). Anterior is up; scale bar = 100 μm. (*F-J*) PGC cluster quantifications of each eRNAi treatment (G-J) compared to (F) *DsRed* controls. Red asterisks denote significant size differences of PGC clusters in that segment compared to controls. Black dots denote significant differences in presence/absence of PGC clusters compared to controls. Numbers below each bar correspond to the number of hemisegments scored. (*K*) Box plot showing the distribution of total PGC volumes per embryo in each knockdown condition and the control condition (grey). Red asterisks denote significance levels resulting from a Mann-Whitney test. The whiskers extend to data points that are 1.5 times above the interquartile range away from the first or third quartile. The black lines represent the medians. n= the number of embryos observed for each condition. (*L*) 100% stacked bar chart showing the proportion of eRNAi embryos displaying

homeotic phenotypes. Ax = abdominal segment x; St. = embryonic stage (62). All P-values for each test are listed in Tables *S2 and S4*. */•P<0.05, **/••P<0.01, ***/•••P<0.001.

Fig. 3. Double eRNAi reveals synergistic effects of Hox repression on germ cells. (*A-C*) PGC cluster quantifications of each eRNAi treatment. Asterisks denote significant size differences from *DsRed* controls (see Fig, 2F) and single eRNAi treatments (Fig. 2H-J) in that segment; asterisk colors indicate comparisons to *DsRed* (black), *Gb-Antp* eRNAi (dark blue), *Gb-abd-A* eRNAi (light purple), or *Gb-Ubx* eRNAi (dark purple). Numbers below each bar correspond to the number of hemisegments scored. (*D*) Box plot showing the distribution of total PGC volumes per embryo in each knockdown condition and the control condition (grey) except for *Gb-Ubx+Gb-abd-A* eRNAi, which displayed no significant total PGC differences in total (see text). Red asterisks denote significance levels resulting from a Mann-Whitney test. The whiskers extend to data points that are 1.5 times above the interquartile range away from the first or third quartile. The black lines represent the medians. n= the number of embryos observed for each condition. (*E-G*) Bar plots showing the proportion of hemisegments containing PGC clusters in single vs. double eRNAi treatments. The dots represent significance levels; red = compared to *DsRed* control; black = comparisons between single and double eRNAi conditions. All P-values for each test are listed in Tables *S3 and S5-S7*. */•P<0.05, **/••P<0.01, ***/•••P<0.001.

Fig. 4. Combinatorial action of Hox genes regulate segmental positions of PGC. (*A*) Summary of the eRNAi results. In wild-type embryos, PGC clusters (red circles) form on A2-A4 (4). Significant changes in PGC number (grey) or appearance of ectopic PGCs (black) in each segment are induced by specific single or double Hox gene knockdowns. (*B*) Proposed mechanisms of combinatorial action of Hox genes on PGC development. Colored bars represent Hox expression domains (Fig. *S3*; (38, 39)). Arrows represent activating functions; and barred arrows represent repressive functions.

Supplementary Materials

Supplementary Materials and Methods

Phylogenetic Analysis

Protein sequences of 119 annotated arthropod Hox gene (Fig. S1) and Distal-less (Dll) orthologues (for use as an outgroup) were retrieved from GenBank. These 119 sequences were used to make an alignment using MUSCLE (63) with eight iterations. The Smart Model Selection program (64) was used to find the best matrix for use in constructing the phylogeny (VT; AIC=164894.36226) and the best "decoration" (+G+I+F; AIC=164894.20896). This model was used with the resulting MUSCLE alignment to construct a maximum likelihood tree using PhyML (65). This resulted in a tree with a log likelihood of -81351.14064 (Fig. *S2*).

Quantitative PCR

Anterior abdominal segments A1-A5 were dissected from control or Hox gene eRNAi-treated embryos (n=5 per treatment for 2.5d and n=3 per treatment for 4d) using fine tungsten needles or fine forceps, and segments were pooled into single tubes. Total RNA was extracted using Trizol (Life Technologies) following the manufacturer's directions. RNA pools were divided into two samples and each half was reverse transcribed to prepare cDNA using SuperScript III (Invitrogen). A no-reverse transcriptase control was performed in parallel for each sample. Each cDNA was divided into three replicate samples and used for qPCR. An MxP3005 machine (Stratagene) was used for qPCR as previously described (5). Relative transcript ratios in the qPCR study were calculated from experiments performed in triplicate and are shown as mean±s.d. in Fig. S4. The housekeeping gene *G. bimaculatus* β*-tubulin* was used as an internal control as previously described (5) . Primers used are listed in Table S8.

Supplementary Figure Legends

Fig. S1. Putative chromosomal arrangement of the *G. bimaculatus* Hox complex. Schematic representation of the Hox complexes of *D. melanogaster* and *G. bimaculatus*. Orthologous genes are shown as color-coded boxes. Dashed rectangle represents genes found in *G. bimaculatus* transcriptome databases but not mapping to the *G. bimaculatus* draft genome database (Taro Mito, University of Tokushima, personal communication). Bar shows scaffold in *G. bimaculatus; gaps indicate regions where scaffold information is unavailable*. Double backslash in *D. melanogaster* cluster indicates the break between the Antennapedia complex and the Bithorax cluster complex. Illustration is not to scale.

Fig. S2. Maximum likelihood phylogeny of all *G. bimaculatus* predicted Hox amino acid sequences and other arthropod Hox amino acid sequences. Orthologous Hox clades are boxed and color-coded as in Figure S1. Distal-less (Dll) protein sequences were used as an outgroup. All nodes with approximate likelihood ratio tests (SH-like) support values with a value greater than or equal to 0.50 are labeled with the support value above the node. The tree resulted from an alignment of 119 arthropod amino acid protein sequences retrieved from GenBank. Protein abbreviations are as follows: Abd-A, Abdominal-A; Abd-B, Abdominal-B; Antp, Antennapedia; Dfd, Deformed; Ftz, Fushi tarazu; Pb, Proboscipedia; Scr, Sex combs reduced; Ubx, Ultrabithorax; Zen, Zerknullt. All prefixes to these Hox proteins denote species names, as follows: Aa, *Aedes albopictus*; Al, *Archegozetes longisetosus*; Am, *Apis mellifera*; Ar, *Athalia rosae*; Bd, *Bacrocera dorsalis*; Bm, *Bombyx mori*; Bt, *Bombus terrestris*; Cc, *Ceratitis capitata*; Cl, *Cimex lectularis*; Cq, *Culex quinquefasciatus*; Cs, *Cupiennius salei*; Daph. mag., *Daphnia magna*; Dc, *Diaphorini citri*; Dm, *Drosophila melanogaster*; Dn, *Diuraphis noxia*; Dp, *Daphnia pulex*; Eb, *Episyrphus balteatus*; Es, *Endeis spinosa*; Gb, *Gryllus bimaculatus*; Hl, *Habropoda laboriosa*; Mq, *Melipona quadrifasciata*; Nv, *Nasonia vitripennis*; Ob, *Operophtera brumata*; Of, *Oncopeltus fasciatus*; Ph, *Parhyale hawaiiensis*; Pm, *Papilio machaon*; Pn, *Paracyclopina nana*; Po, *Phalangium opilio*; Ps, *Pedetontus saltator*; Pt, *Parasteatoda tepidariorum*; Px, *Plutella xylostella*; Rz, *Rhagoletis zephyria*; Sc, *Stomoxys calcitrans*; Tc, *Tribolium castaneum*; Td, *Thermobia domestica*; Tm, *Tenebrio molitor*; Tz, *Trachymyrmex zeteki*; Zn, *Zootermopsis nevadensis*.

Fig. S3. Expression of *Gb-Scr*, *Gb-Antp*, *Gb-Ubx* and *Gb-abd-A* transcripts during *G. bimaculatus* development. Fluorescent *in situ* hybridization of wild type embryos at egg stage (ES) ES7 (A, C, E ,G) and ES8.5 (B, D, F, H). Egg staging as described in (62). Scale bar in A = 500 µm for all panels.

Fig. S4. Validation of eRNAi knockdown via qPCR. Quantitative PCR was conducted to evaluate the efficacy of eRNAi-mediated knockdown against Hox genes in embryos at 2.5 days (d) and 4d after egg laying (AEL). At 2.5d AEL, PGC formation begins and at 4d AEL, PGC clusters are formed (4). Bars show relative expression levels normalized to *Gb-beta-tubulin*. eRNAi against all examined Hox genes reduced their transcript levels, if not at 2.5d AEL then by 4d AEL. Error bars show standard deviation.

Fig. S5. Homeotic transformations resulting from Hox eRNAi. (A) Example of an embryonic stage (St.) St.9 *DsRed* eRNAi control embryo showing the wild-type morphology, with pleuropodia (Pp) on the first abdominal segment (A1). (B) *Gb-Ubx* eRNAi resulted in the transformation of the pleuropodia into ectopic legs (eL4) on A1. (C) *Gb-abd-A* eRNAi resulted in the formation of ectopic pleuropodia-like appendages (arrowheads) on segments A2-A9. (D) Double eRNAi targeting *Gb-Antp* and *Gb-Ubx* resulted in the formation of ectopic legs (eL4) on A1. (E) Double eRNAi targeting *Gb-Ubx* and *Gb-abd-A* resulted in leg-like appendages (arrowheads) forming on segments A1-A9. Scale bars = 100 µm. All images are projections of optical confocal sections of embryos stained with Hoechst.

Fig. S6. Expression patterns of *G. bimaculatus Distal-less* (*Gb-Dll*) and *tramtrack* (*Gb-ttk*) in *Gb-Ubx* and *Gb-abdominal-A* eRNAi embryos. (A-D) *In situ* hybridization for *Gb-Dll* in Hox eRNAi embryos compared with *DsRed* eRNAi control. (A) *Gb-Dll* expression in wild type embryos is detectable in appendages; thoracic legs and pleuropodia (A1) are visible in the figure. (B) *Gb-Ubx* eRNAi embryo shows enlargement of A1 appendage with distally localized *Gb-Dll* expression in the transformed structure. (C) *Gb-abd-A* eRNAi embryo shows ectopic extrusions (marked by yellow dotted lines) in A2-A6 segments. Ectopic *Gb-Dll* expression is detected in these extrusions. (D) Sense RNA probe against *Gb-Dll* used as negative *in situ* control in *DsRed* embryos. (E-H) *In situ* hybridization for *Gb-ttk* in Hox eRNAi

528 embryos compared with *DsRed* eRNAi control. (E) *Gb-ttk* transcripts are enriched in pleuropodia, and
529 low-level expression is also detectable throughout the entire embryo in *DsRed* eRNAi controls. (F) *Gb-*
530 *Ubx* eRNAi embryo shows reduced expression in pleuropodia and slightly increased expression in the
531 rest of the abdomen. (G) In *Gb-abd-A e*RNAi embryos *Gb-ttk* expression are lost from ectopic abdominal
532 extrusions and nearly entirely from the rest of the embryo. (H) Sense RNA probe against *Gb-ttk* used as
533 negative *in situ* control in *DsRed* embryos. Ax: abdominal segment x; eL4: ectopic 4th leg; Pp:
534 pleuropodia; T3: 3rd thoracic leg. Scale bar = 100 μm for all panels.
535
536 **Fig. S7**. **Statistical comparisons of PGC volumes from eRNAi embryos with and without homeotic**
537 **phenotypes.** (A) *Gb-Ubx*, (B) *Gb-abd-A* (C) *Gb-Antp*+*Gb-Ubx* and (D) *Gb-Ubx*+*Gb-abd-A* eRNAi
538 knockdowns. In each condition, the distributions of the total PGC numbers per embryo were not
539 statistically different between embryos with homeotic phenotypes and those without. The whiskers extend
540 to data points that are 1.5 times above the interquartile range away from the first or third quartile. The
541 black lines represent the medians. n= the number of embryos observed for each condition. P-values for
542 (A-C) were based on the Mann-Whitney Test, and the P-value for (D) is based on a t-test due to the low
543 number of samples in this comparison.
544
545 **Fig. S8. Expression of *G. bimaculatus eyes-absent* (*Gb-eya*) and *Six4* (*Gb-Six4*) in PGC**
546 **development.** (A-D') *Gb-eya* transcripts are detectable at highest levels in the eye and brain primordia,
547 and in the appendages in ring-like patterns. (B-B') High magnification view of the abdominal region boxed
548 in red in (A) shows that *Gb-eya* is expressed in each abdominal coelomic pouch, but not obviously at high
549 levels in or adjacent to PGCs (marked by yellow dotted lines and labeled with anti-Gb-Piwi (B')). (C, D)
550 Sense RNA probe against *Gb-eya* was used as a negative *in situ* hybridization control. (E-H') *Gb-Six4*
551 transcripts are detected throughout the entire embryo, with increased expression in the thoracic coelomic
552 pouches. (F-F') High magnification view of the abdominal region boxed in red in (E) shows no enriched
553 *Gb-Six-4* expression in or around PGCs. Scale bar = 500 μm in A, C, E, G and 100 μm in B, applicable to
554 B-H'.

555 **Supplementary Tables**

556

557 **Table S1:** Embryonic RNAi injection statistics.

558

559 **Table S2:** Mann-Whitney U test statistics on PGC measurements for single eRNAi treatments.

560

561 **Table S3:** Mann-Whitney U test statistics on PGC measurements for double eRNAi treatments.

562

563 **Table S4:** Statistical tests of presence/absence of PGC clusters in single Hox eRNAi treatments.

564

565 **Table S5:** Statistical tests of presence/absence of PGC clusters in double Hox eRNAi treatments.

566

567 **Table S6**: Mann-Whitney U test statistics on PGC measurements for single vs. double eRNAi treatments.

568

569 **Table S7:** Statistical tests of presence/absence of PGC clusters in single vs. double Hox eRNAi

570 treatments.

571

572 **Table S8**: Primers used for gene cloning and qPCR.

573

Figure 1
Barnett, Nakamura & Extavour

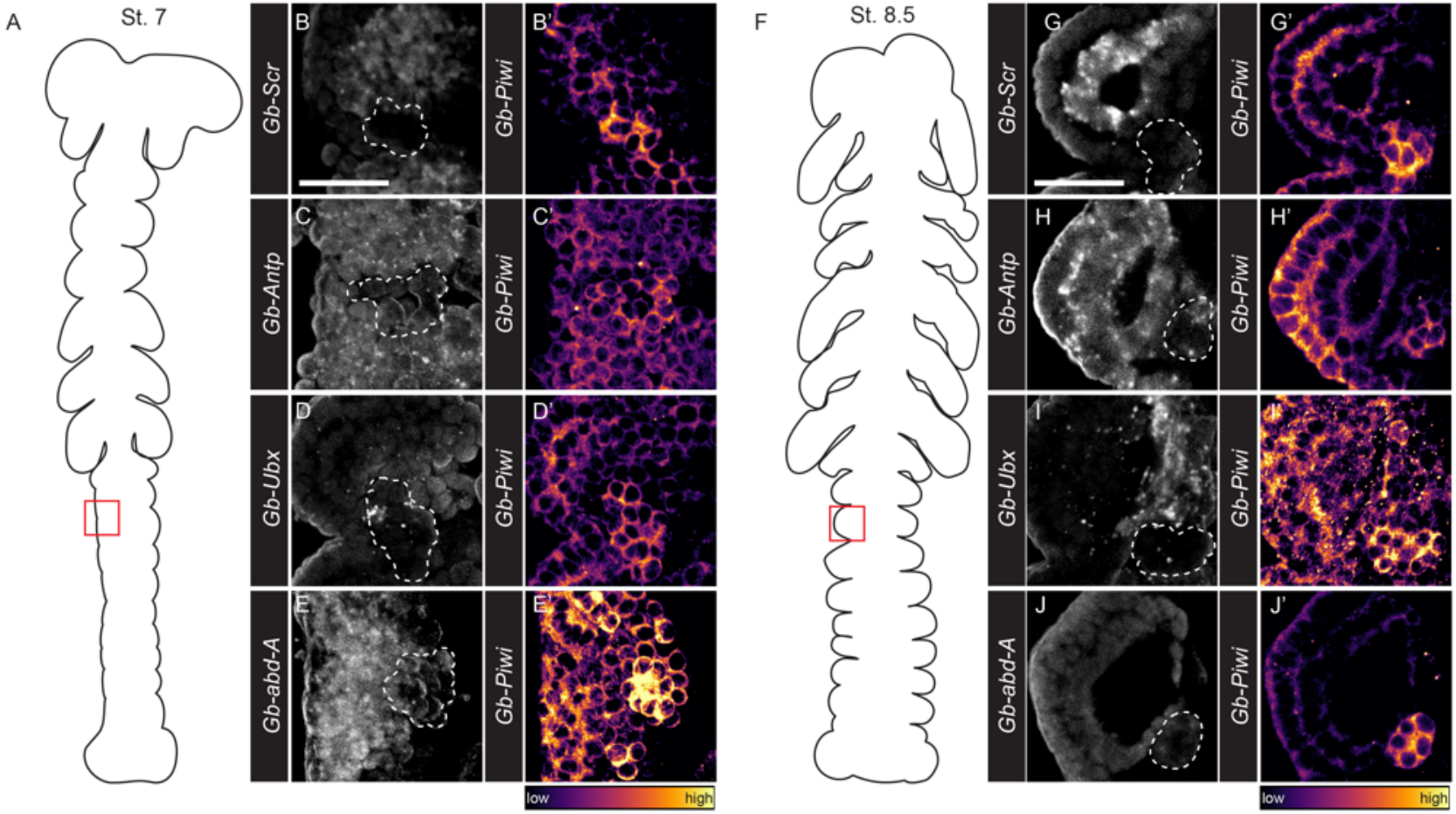

Figure 2
Barnett, Nakamura & Extavour

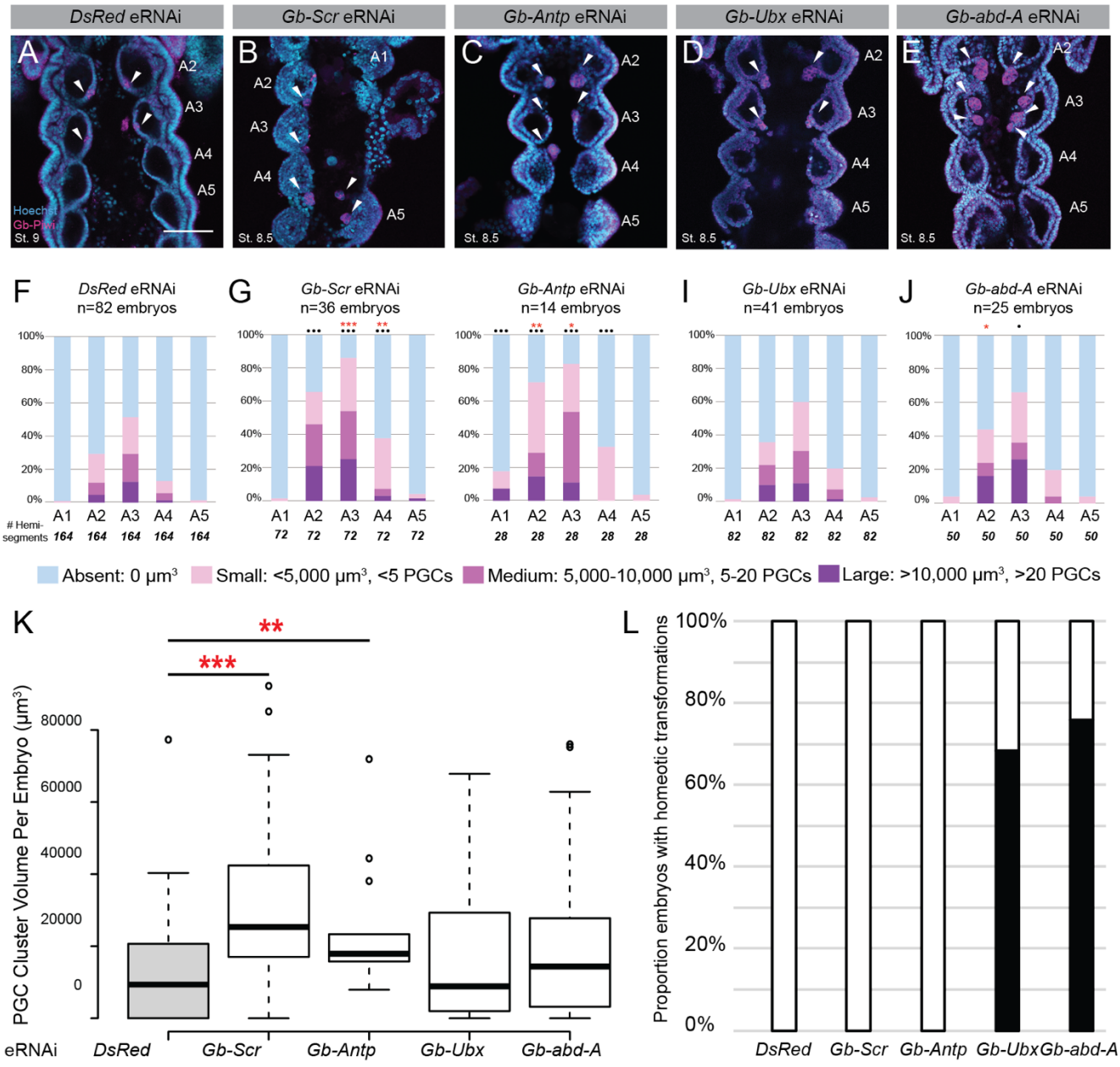

Figure 3
Barnett, Nakamura & Extavour

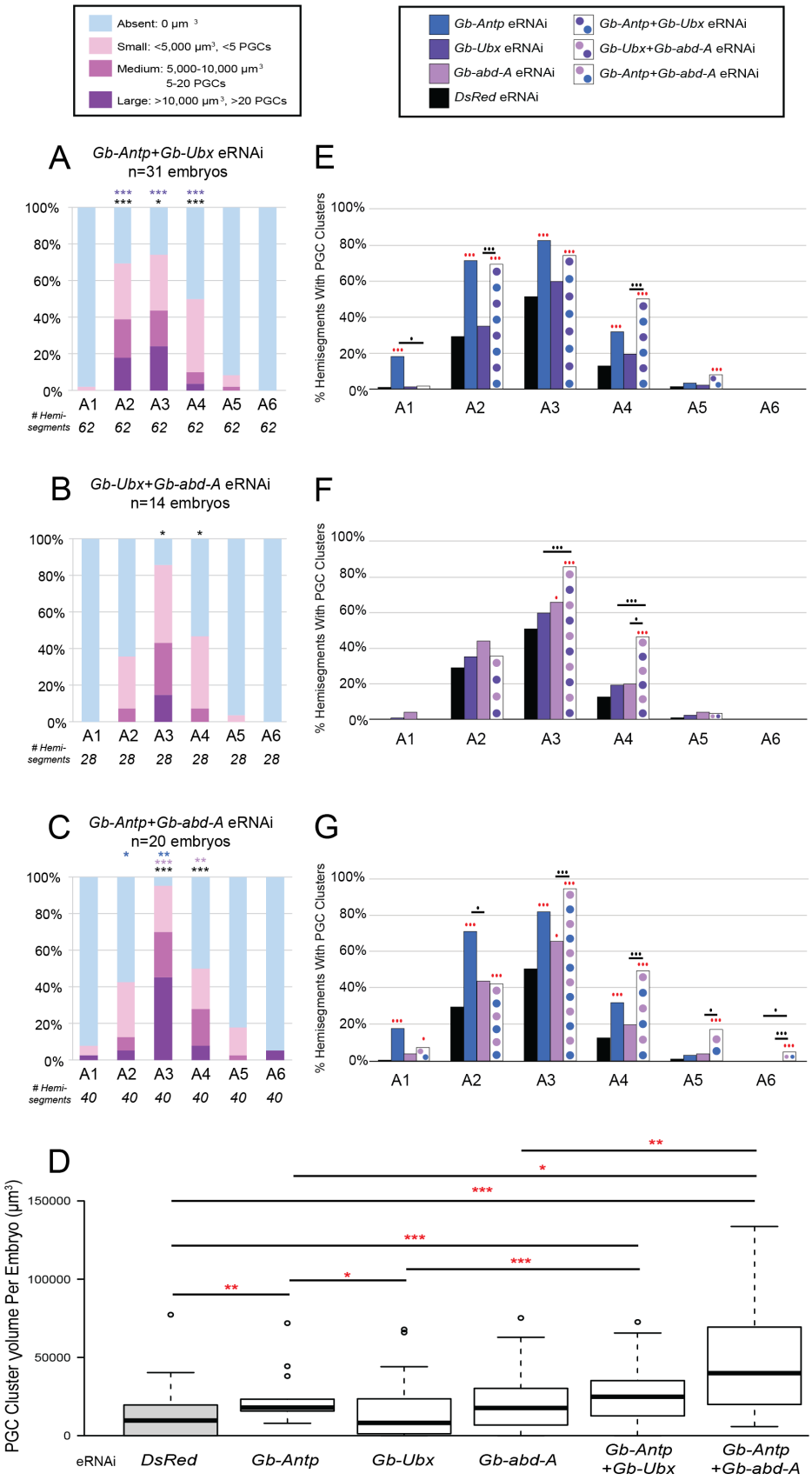

Figure 4
Barnett, Nakamura & Extavour

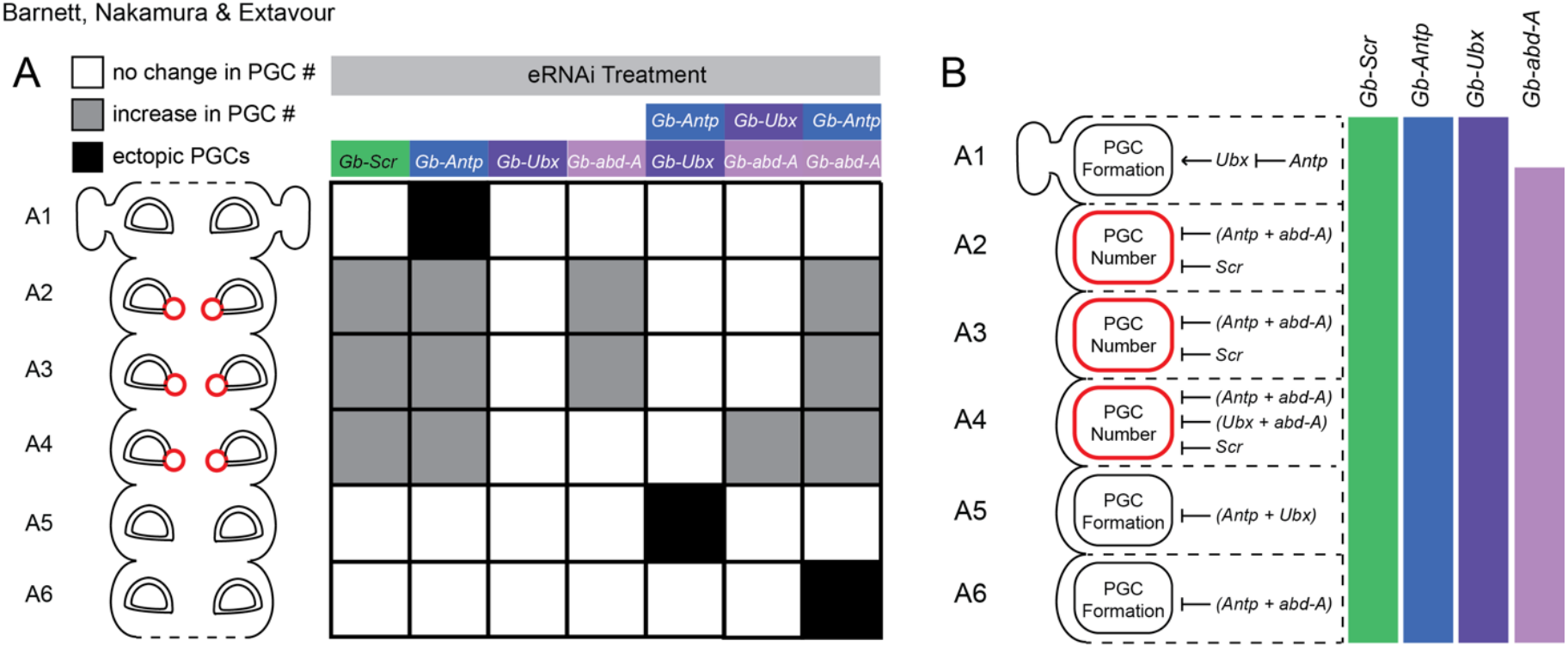

Figure S1
Barnett, Nakamura & Extavour

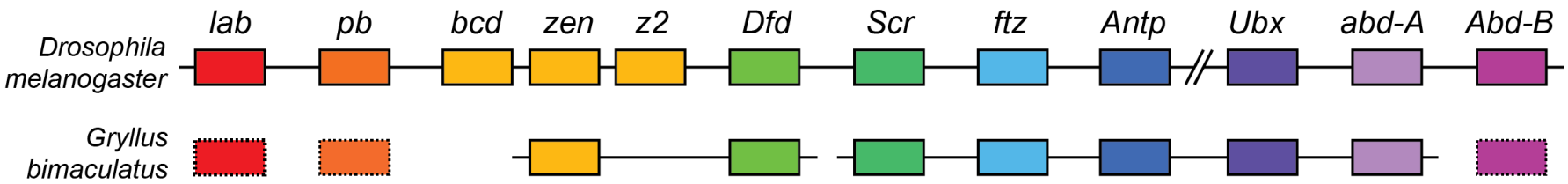

Figure S2
Barnett, Nakamura & Extavour

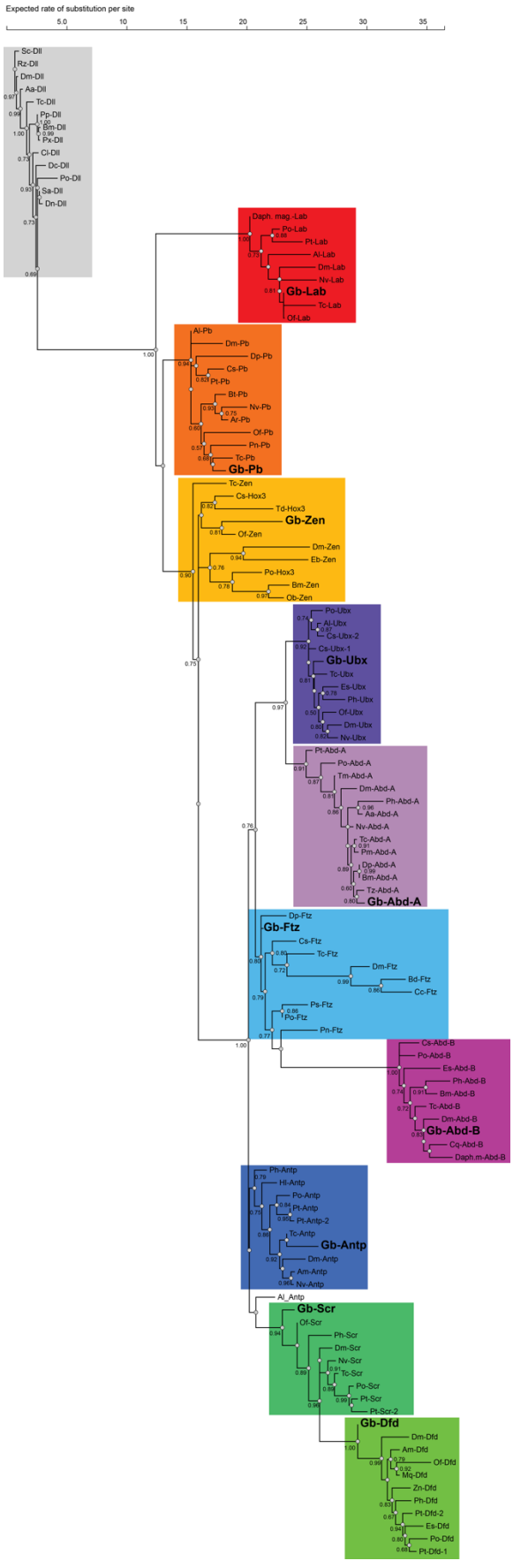

Figure S3
Barnett, Nakamura & Extavour

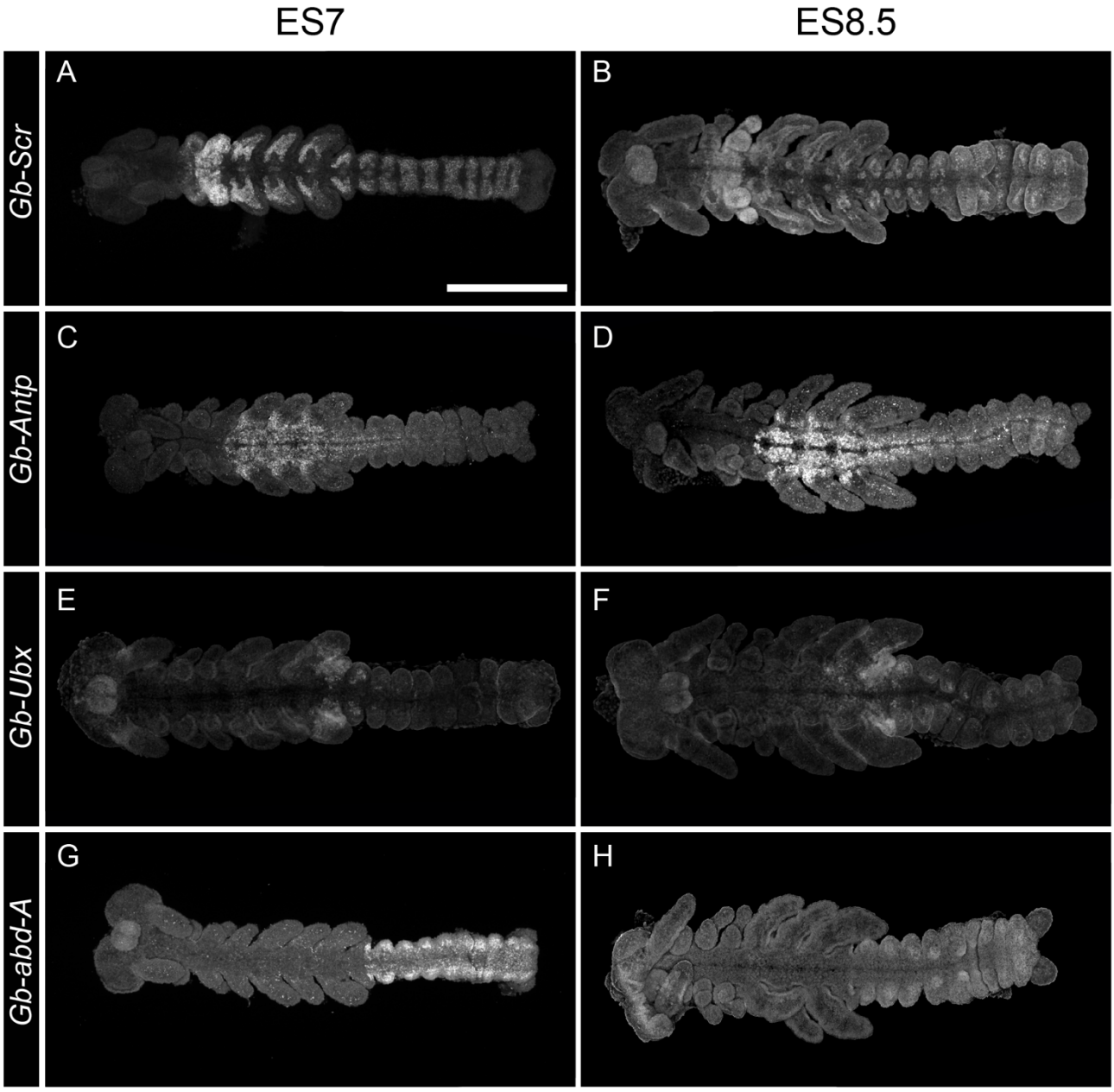

Figure S4
Barnett, Nakamura & Extavour

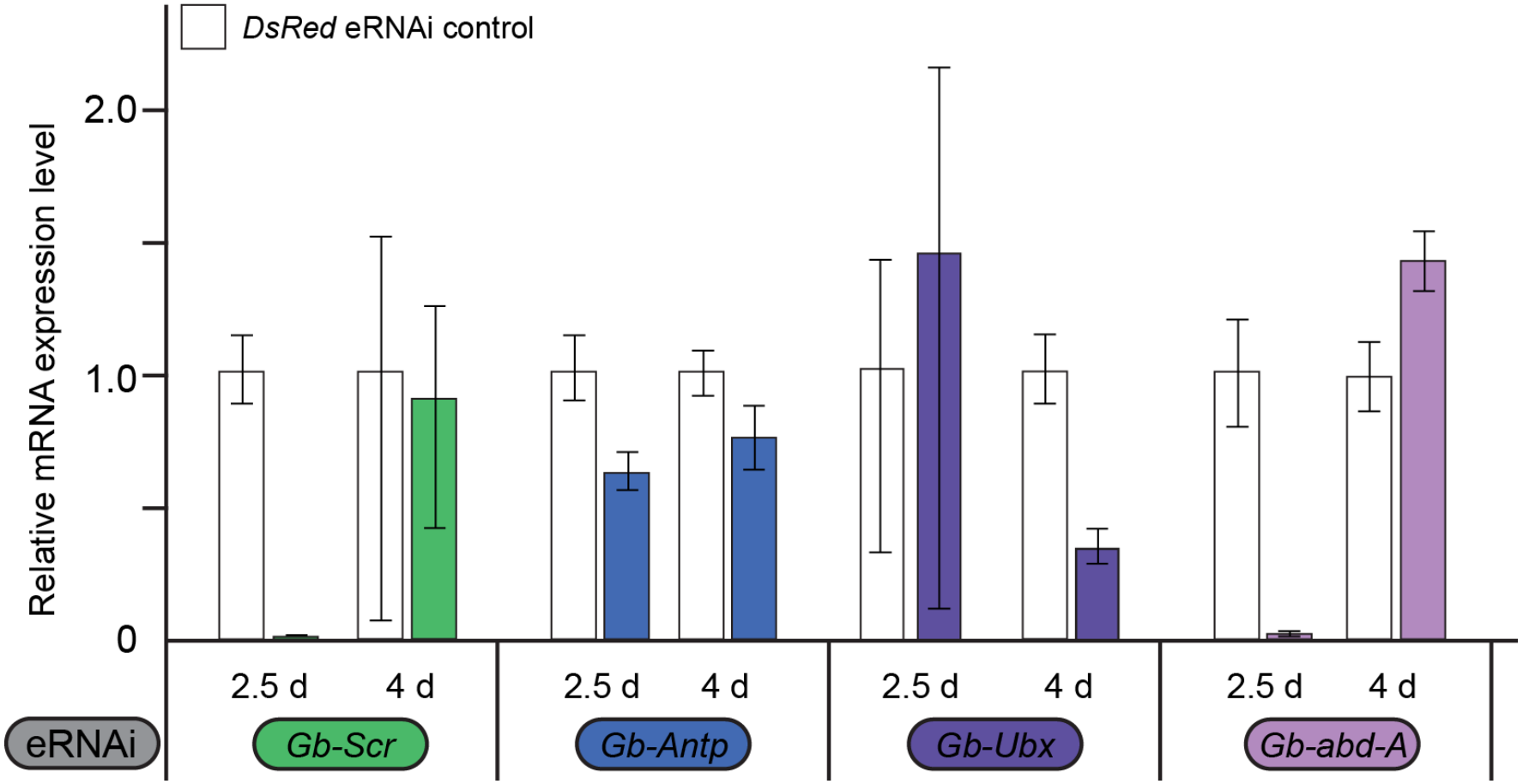

Figure S5
Barnett, Nakamura & Extavour

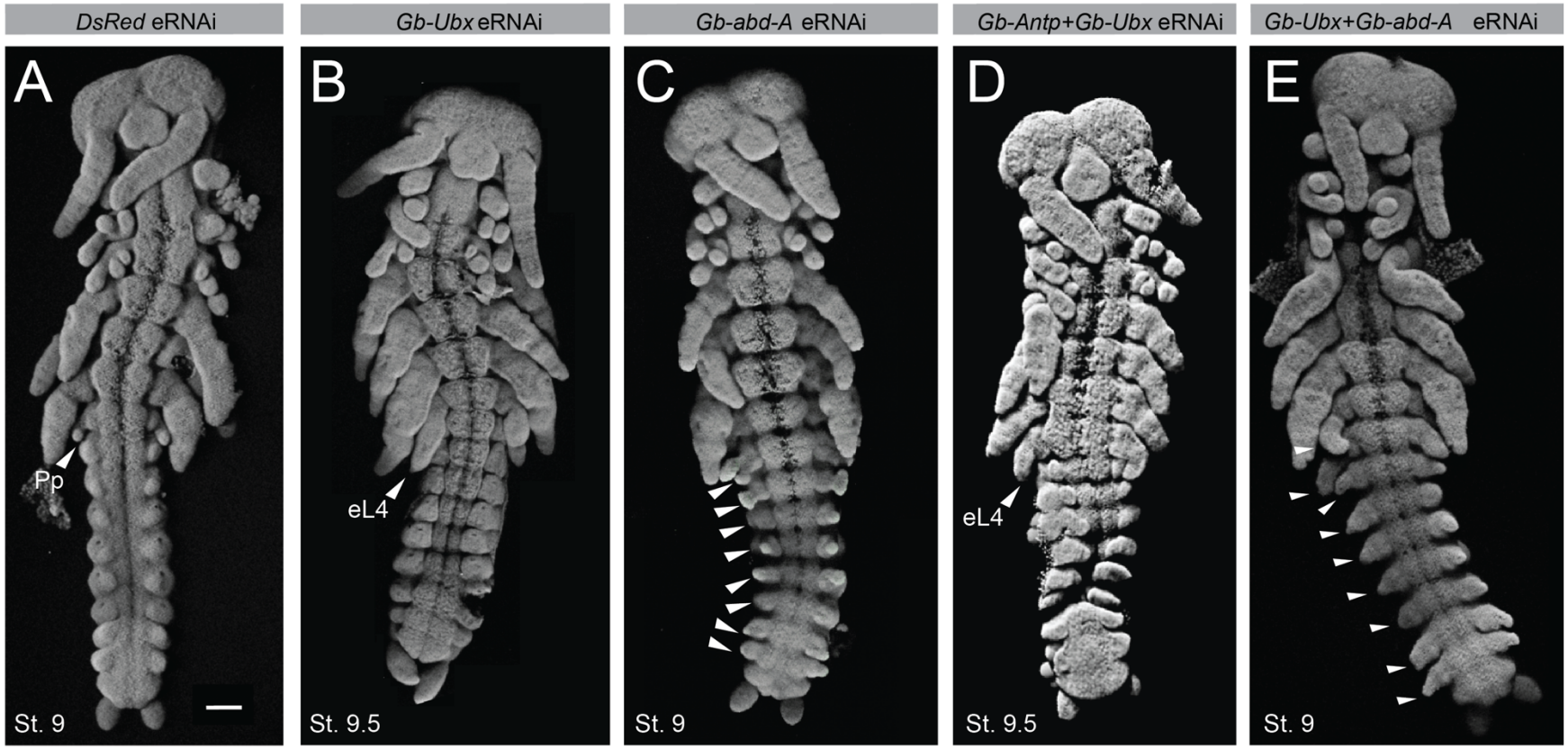

Figure S6
Barnett, Nakamura & Extavour

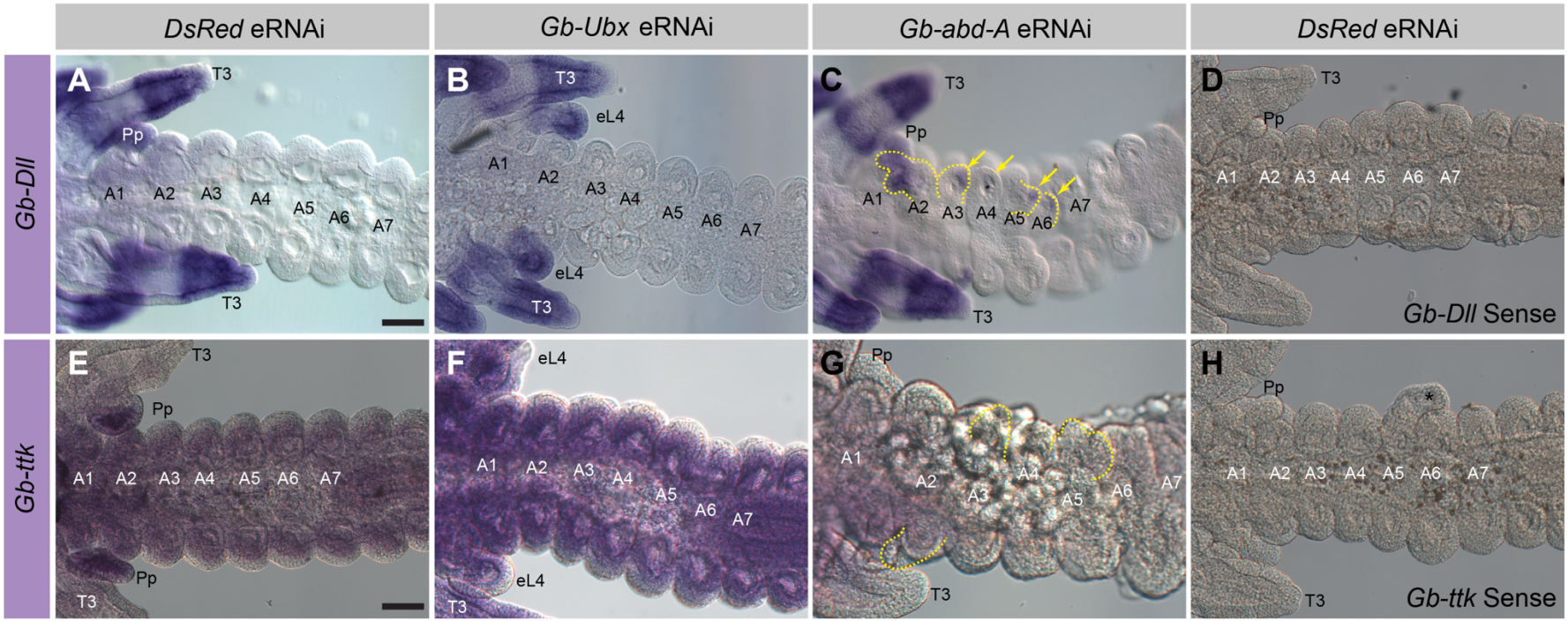

Figure S7
Barnett, Nakamura & Extavour

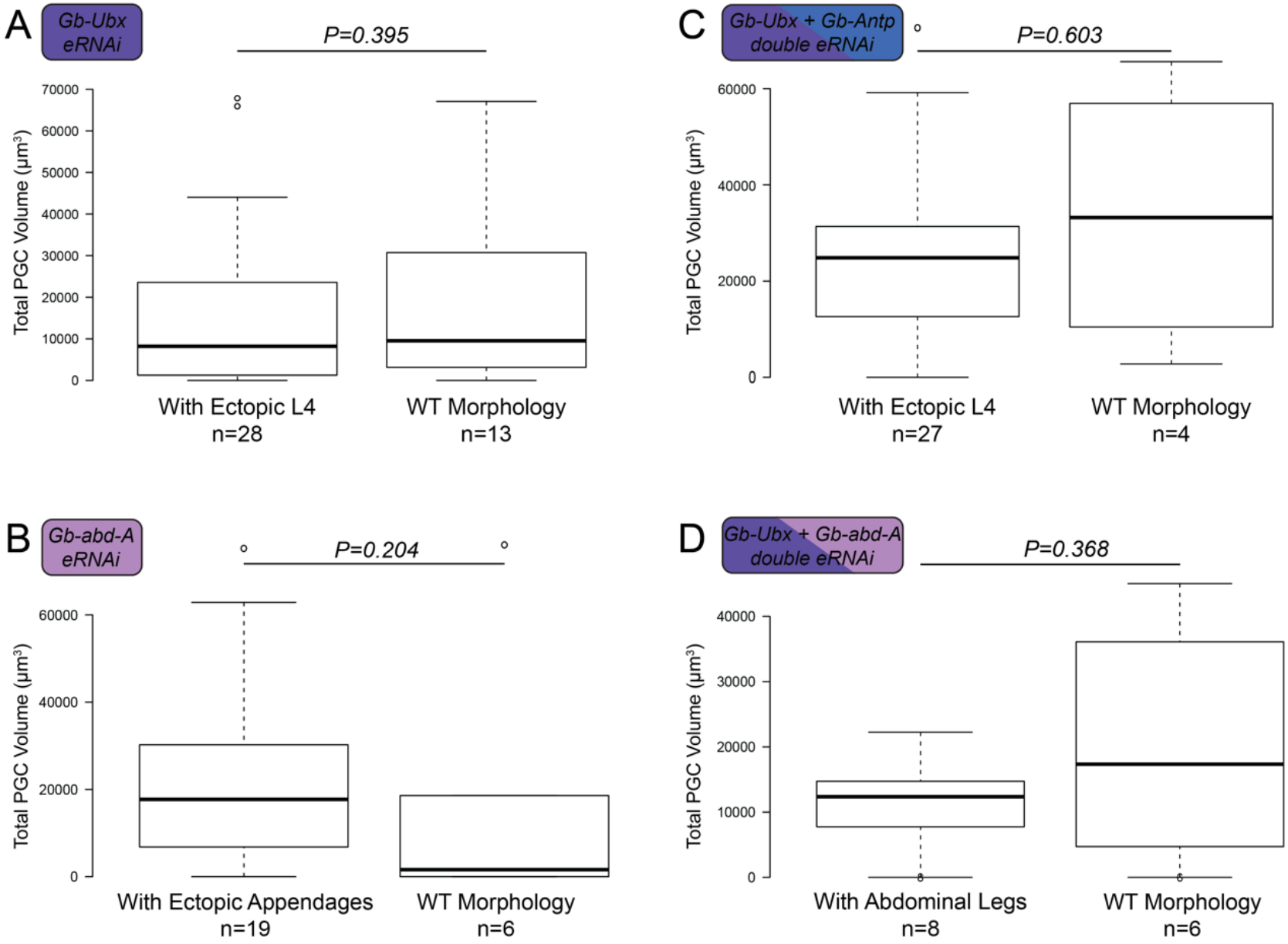

Figure S8
Barnett, Nakamura & Extavour

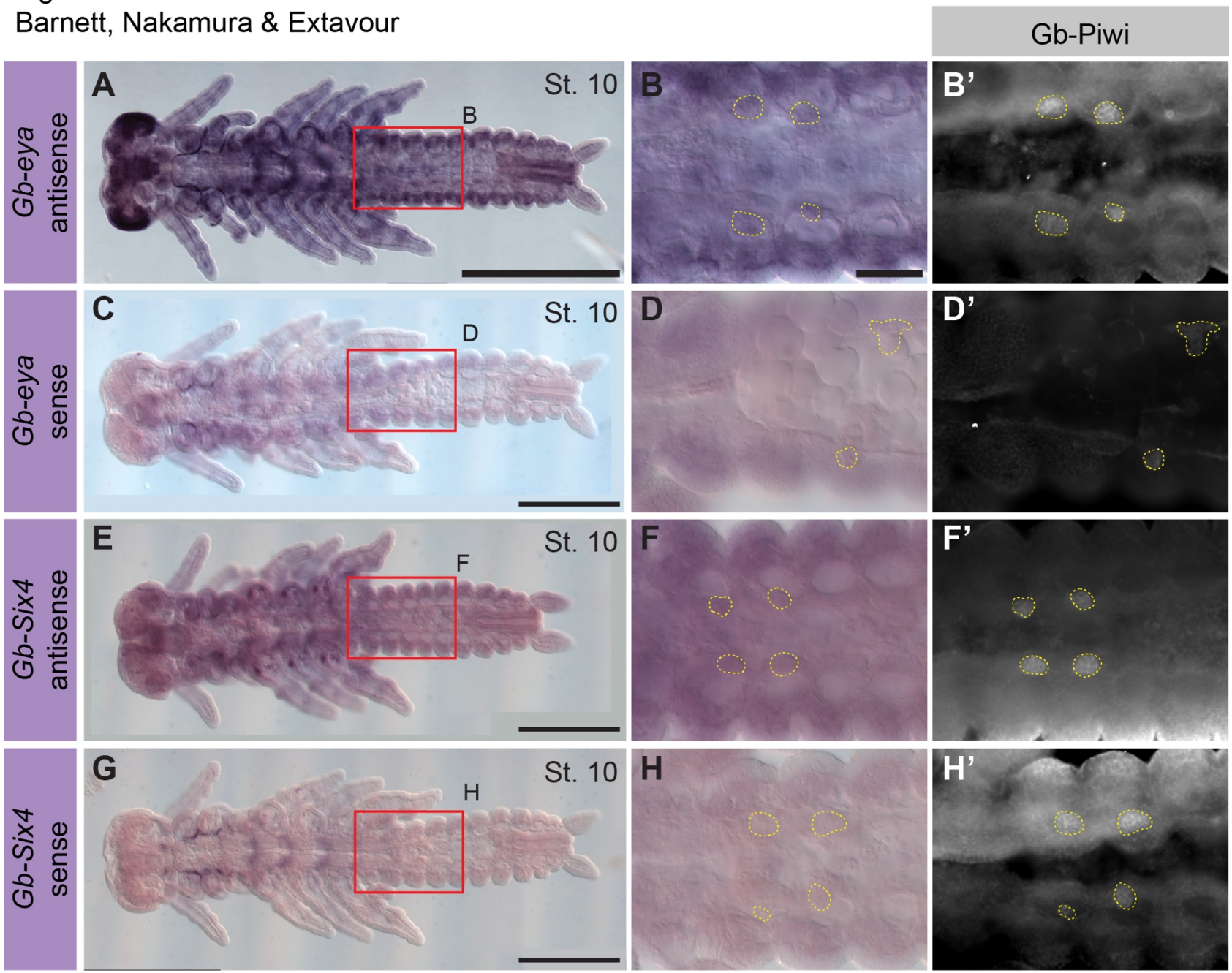

Table S1: Embryonic RNAi Injection statistics.

Injectant	Concentration	# Embryos Injected	# (%) Embryos Survived Injection to Stage 8	# Embryos scored for PGCs in segments A1-A5
DsRed dsRNA	6 µg/µl	3,190	1,395 (43.7)	66
	9 µg/µl	417	176 (42.2)	16
Gb-Scr dsRNA	6 µg/µl	344	175 (50.9)	36
Gb-Antp dsRNA	6 µg/µl	1,103	251 (22.8)	14
Gb-Ubx dsRNA	6 µg/µl	203	163 (80.3)	29
	9 µg/µl	372	112 (30.1)	12
Gb-abd-A dsRNA	6 µg/µl	1,126	375 (33.3)	16
	8 µg/µl	149	22 (14.8)	9
Gb-Scr/abd-A RNAi	3 µg/µl each	268	0 (0)	0
Gb-Scr/Antp RNAi	3 µg/µl each	243	0 (0)	0
Gb-Antp/Ubx dsRNA	3 µg/µl each	374	201 (53.7)	31
Gb-Antp/abd-A dsRNA	3 µg/µl each	330	142 (43.0)	20
Gb-Ubx/abd-A dsRNA	3 µg/µl each	192	84 (43.8)	14

Table S2: Mann-Whitney U test statistics on PGC measurements for single eRNAi treatments. A1-5, abdominal segments 1-5.

Comparison	U Value	Z Score	P-Value	Significant?
Gb-Scr VS. DsRed A1	5858.5	-0.0931	0.9282	No
Gb-Scr VS. DsRed A2	3330.0	-5.3290	< .00001	Yes
Gb-Scr VS. DsRed A3	3714.5	-4.5328	< .00001	Yes
Gb-Scr VS. DsRed A4	4570.0	-2.7613	0.0057	Yes
Gb-Scr VS. DsRed A5	5730.0	-0.3592	0.7188	No
Gb-Scr VS. DsRed Total	691.0	-4.5851	< .00001	Yes
Gb-Antp VS. DsRed A1	1900.5	-1.4534	0.1470	No
Gb-Antp VS. DsRed A2	1316.0	-3.6042	0.0032	Yes
Gb-Antp VS. DsRed A3	1712.0	-2.1471	0.0315	Yes
Gb-Antp VS. DsRed A4	1900.5	-1.4534	0.1470	No
Gb-Antp VS. DsRed A5	2241.0	-0.2005	0.8414	No
Gb-Antp VS. DsRed Total	311.0	-2.7249	0.0065	Yes
Gb-Ubx VS. DsRed A1	6518.5	-0.0792	0.9362	No
Gb-Ubx VS. DsRed A2	6078.0	-1.2269	0.2187	No
Gb-Ubx VS. DsRed A3	6349.5	-0.7108	0.4777	No
Gb-Ubx VS. DsRed A4	6299.0	-0.8068	0.4179	No
Gb-Ubx VS. DsRed A5	6553.0	-0.0893	0.9282	No
Gb-Ubx VS. DsRed Total	1513.0	-0.8986	0.3681	No
Gb-abd-A VS. DsRed A1	3962.0	-0.3587	0.7188	No
Gb-abd-A VS. DsRed A2	3325.0	-2.0206	0.0433	Yes
Gb-abd-A VS. DsRed A3	3450.0	-1.6945	0.0910	No
Gb-abd-A VS. DsRed A4	3839.0	-0.6796	0.4965	No
Gb-abd-A VS. DsRed A5	3988.0	-0.2909	0.7718	No
Gb-abd-A VS. DsRed Total	818.0	-1.5202	0.1285	No

Table S3: Mann-Whitney U test statistics on PGC measurements for double eRNAi treatments. A1-5, abdominal segments 1-5.

Comparison	U Value	Z Score	P-Value	Significant?
(Gb-Antp+Gb-Ubx) VS. DsRed A1	5033.5	-0.1140	0.9124	No
(Gb-Antp+Gb-Ubx) VS. DsRed A2	2820.0	-5.1610	< .00001	Yes
(Gb-Antp+Gb-Ubx) VS. DsRed A3	3756.0	-3.0268	0.0024	Yes
(Gb-Antp+ Gb-Ubx) VS. DsRed A4	3331.5	-3.9947	0.0001	Yes
(Gb-Antp+ Gb-Ubx) VS. DsRed A5	4734.0	-0.7969	0.4237	No
(Gb-Antp+ Gb-Ubx) VS. DsRed Total	660.0	-3.9285	0.0001	Yes
(Gb-Ubx+ Gb-abd-A) VS. DsRed A1	2282.0	0.0496	0.9601	No
(Gb-Ubx+ Gb-abd-A) VS. DsRed A2	2204.0	-0.3366	0.7279	No
(Gb-Ubx+ Gb-abd-A) VS. DsRed A3	1755.0	-1.9888	0.0466	Yes
(Gb-Ubx+ Gb-abd-A) VS. DsRed A4	1598.5	-2.5647	0.0105	Yes
(Gb-Ubx+ Gb-abd-A) VS. DsRed A5	2243.0	-0.1931	0.8493	No
(Gb-Ubx+ Gb-abd-A) VS. DsRed Total	492.0	-0.8460	0.3953	No
(Gb-Antp+ Gb-abd-A) VS. DsRed A1	3054.5	-0.6721	0.5029	No
(Gb-Antp+ Gb-abd-A) VS. DsRed A2	2928.5	-1.0485	0.2937	No
(Gb-Antp+ Gb-abd-A) VS. DsRed A3	1319.0	-5.8563	< .00001	Yes
(Gb-Antp+ Gb-abd-A) VS. DsRed A4	2040.0	-3.7026	0.0002	Yes
(Gb-Antp+ Gb-abd-A) VS. DsRed A5	2744.0	-1.5996	0.1096	No
(Gb-Antp+ Gb-abd-A) VS. DsRed A6	3116.0	-0.4884	0.6241	No
(Gb-Antp+ Gb-abd-A) VS. DsRed Total	224.0	-5.0191	< .00001	Yes

Table S4: Statistical tests of presence/absence of PGC clusters in single Hox eRNAi treatments. FE = Fisher's Exact Test; X2 = Chi-Square Test; N/A = not applicable; A1-5, abdominal segments 1-5.

Comparison	Test	X2 Statistic	P-Value	Significant?
Gb-Scr VS. DsRed A1	FE	N/A	0.518	No
Gb-Scr VS. DsRed A2	X2	26.976	< .00001	Yes
Gb-Scr VS. DsRed A3	X2	25.818	< .00001	Yes
Gb-Scr VS. DsRed A4	X2	18.832	0.000	Yes
Gb-Scr VS. DsRed A5	FE	N/A	0.168	No
Gb-Antp VS. DsRed A1	FE	N/A	0.000	Yes
Gb-Antp VS. DsRed A2	X2	18.585	0.000	Yes
Gb-Antp VS. DsRed A3	X2	9.269	0.002	Yes
Gb-Antp VS. DsRed A4	X2	6.784	0.009	Yes
Gb-Antp VS. DsRed A5	FE	N/A	0.271	No
Gb-Ubx VS. DsRed A1	FE	N/A	1.000	No
Gb-Ubx VS. DsRed A2	X2	0.945	0.331	No
Gb-Ubx VS. DsRed A3	X2	1.604	0.205	No
Gb-Ubx VS. DsRed A4	X2	1.924	0.165	No
Gb-Ubx VS. DsRed A5	FE	N/A	0.602	No
Gb-abd-A VS. DsRed A1	FE	N/A	0.137	No
Gb-abd-A VS. DsRed A2	FE	N/A	0.059	No
Gb-abd-A VS. DsRed A3	X2	4.362	0.037	Yes
Gb-abd-A VS. DsRed A4	X2	1.601	0.206	No
Gb-abd-A VS. DsRed A5	FE	N/A	0.137	No

Table S5: Statistical tests of presence/absence of PGC clusters in double Hox eRNAi treatments. FE = Fisher's Exact Test; X2 = Chi-Square Test; N/A = not applicable; A1-6, abdominal segments 1-6.

Comparison	Test	X2 Statistic	P-Value	Significant?
(Gb-Antp+ Gb-Ubx) VS. DsRed A1	FE	N/A	0.4743	No
(Gb-Antp+ Gb-Ubx) VS. DsRed A2	X2	30.0584	< .00001	Yes
(Gb-Antp+ Gb-Ubx) VS. DsRed A3	X2	9.7186	0.0018	Yes
(Gb-Antp+ Gb-Ubx) VS. DsRed A4	X2	35.1369	< .00001	Yes
(Gb-Antp+ Gb-Ubx) VS. DsRed A5	FE	N/A	0.0065	Yes
(Gb-Ubx+ Gb-abd-A) VS. DsRed A1	FE	N/A	1.0000	No
(Gb-Ubx+ Gb-abd-A) VS. DsRed A2	X2	0.4714	0.4923	No
(Gb-Ubx+ Gb-abd-A) VS. DsRed A3	FE	N/A	0.0007	Yes
(Gb-Ubx+ Gb-abd-A) VS. DsRed A4	X2	18.5549	0.0000	Yes
(Gb-Ubx+ Gb-abd-A) VS. DsRed A5	FE	N/A	0.2710	No
(Gb-Antp+ Gb-abd-A) VS. DsRed A1	FE	N/A	0.0244	Yes
(Gb-Antp+ Gb-abd-A) VS. DsRed A2	X2	11.2953	0.0008	Yes
(Gb-Antp+ Gb-abd-A) VS. DsRed A3	X2	25.6402	< .00001	Yes
(Gb-Antp+ Gb-abd-A) VS. DsRed A4	X2	24.5565	< .00001	Yes
(Gb-Antp+ Gb-abd-A) VS. DsRed A5	FE	N/A	0.0000	Yes
(Gb-Antp+ Gb-abd-A) VS. DsRed A6	FE	N/A	0.0000	Yes

Table S6: Mann-Whitney U test statistics on PGC measurements for single vs. double eRNAi treatments. A1-6, abdominal segments 1-6.

Comparison	U Value	Z Score	P-Value	Significant?
(Gb-Antp+ Gb-Ubx) VS. Gb-Antp A1	759.0	-1.18816	0.234	No
(Gb-Antp+ Gb-Ubx) VS. Gb-Antp A2	811.0	0.49243	0.624	No
(Gb-Antp+ Gb-Ubx) VS. Gb-Antp A3	834.0	0.29197	0.772	No
(Gb-Antp+ Gb-Ubx) VS. Gb-Antp A4	709.5	1.37706	0.168	No
(Gb-Antp+ Gb-Ubx) VS. Gb-Antp A5	829.5	0.33119	0.741	No
(Gb-Antp+ Gb-Ubx) VS. Gb-Antp Total	194.0	0.55163	0.582	No
(Gb-Antp+ Gb-Ubx) VS. Gb-Ubx A1	2470.5	-0.03702	0.968	No
(Gb-Antp+ Gb-Ubx) VS. Gb-Ubx A2	1764.5	-3.13491	0.002	Yes
(Gb-Antp+ Gb-Ubx) VS. Gb-Ubx A3	1997.5	-2.19484	0.028	Yes
(Gb-Antp+ Gb-Ubx) VS. Gb-Ubx A4	1824.5	-2.89283	0.004	Yes
(Gb-Antp+ Gb-Ubx) VS. Gb-Ubx A5	2339.0	-0.57791	0.562	No
(Gb-Antp+ Gb-Ubx) VS. Gb-Ubx Total	399.0	-2.68391	0.007	Yes
(Gb-Ubx+ Gb-abd-A) VS. Gb-Ubx A1	1106.0	0.09464	0.928	No
(Gb-Ubx+ Gb-abd-A) VS. Gb-Ubx A2	1063.0	0.57983	0.562	No
(Gb-Ubx+ Gb-abd-A) VS. Gb-Ubx A3	944.0	-1.39639	0.162	No
(Gb-Ubx+ Gb-abd-A) VS. Gb-Ubx A4	864.0	-1.94534	0.0511	Approaching
(Gb-Ubx+ Gb-abd-A) VS. Gb-Ubx A5	1109.0	-0.07361	0.944	No
(Gb-Ubx+ Gb-abd-A) VS. Gb-Ubx Total	258.0	-0.55066	0.582	No
(Gb-Ubx+ Gb-abd-A) VS. Gb-abd-A A1	672.0	0.28645	0.772	No
(Gb-Ubx+ Gb-abd-A) VS. Gb-abd-A A2	586.0	1.18225	0.238	No
(Gb-Ubx+ Gb-abd-A) VS. Gb-abd-A A3	658.5	-0.42707	0.667	No
(Gb-Ubx+ Gb-abd-A) VS. Gb- abd-A A4	531.0	-1.75514	0.078	No
(Gb-Ubx+ Gb-abd-A) VS. Gb-abd-A A5	697.0	0.02604	0.976	No
(Gb-Ubx+abd-A) VS. Gb-abd-A Total	163.0	0.33669	0.728	No
(Gb-abd-A+ Gb-Antp) VS. Gb-abd-A A1	610.5	0.32864	0.741	No
(Gb-abd-A+ Gb-Antp) VS. Gb-abd-A A2	891.0	0.88102	0.379	No
(Gb-abd-A+ Gb-Antp) VS. Gb-abd-A A3	518.0	-3.90977	0.000	Yes
(Gb-abd-A+ Gb-Antp) VS. Gb-abd-A A4	661.0	-2.74861	0.006	Yes
(Gb-abd-A+ Gb-Antp) VS. Gb- abd-A A5	858.0	-1.14898	0.250	No
(Gb-abd-A+ Gb-Antp) VS. Gb-abd-A A6	950.0	-0.40194	0.689	No
(Gb-abd-A+ Gb-Antp) VS. Gb- abd-A Total	115.0	-3.0722	0.002	Yes
(Gb-abd-A+ Gb-Antp) VS. Gb-Antp A1	523.0	-0.68685	0.490	No
(Gb-abd-A+ Gb-Antp) VS. Gb-Antp A2	366.0	-2.41123	0.016	Yes
(Gb-abd-A+ Gb-Antp) VS. Gb-Antp A3	305.0	3.17135	0.001	Yes
(Gb-abd-A+ Gb-Antp) VS. Gb-Antp A4	412.0	1.82555	0.067	No
(Gb-abd-A+ Gb-Antp) VS. Gb-Antp A5	483.5	0.94705	0.342	No
(Gb-abd-A+ Gb-Antp) VS. Gb-Antp A6	532.0	0.34268	0.728	No
(Gb-abd-A+ Gb-Antp) VS. Gb-Antp Total	69.0	2.46699	0.013	Yes
Gb-Antp VS. Gb-Ubx Total	177.0	-2.1157	0.034	Yes
Gb-Antp VS. Gb-abd-A Total	140.0	-1.01006	0.312	No
Gb-Ubx VS. Gb- abd-A Total	461.0	-0.67416	0.503	No

Table S7: Statistical tests of presence/absence of PGC clusters in single vs. double Hox eRNAi treatments. FE = Fisher's Exact Test; X2 = Chi-Square Test; NA = not applicable.

Comparison	Test	X2 Statistic	P-Value	Significant?
(Gb-Antp+Gb-Ubx) VS. Antp A1	FE	N/A	0.0103	Yes
(Gb-Antp+Gb-Ubx) VS. Antp A2	X2	0.0395	0.8424	No
(Gb-Antp+Gb-Ubx) VS. Antp A3	X2	0.6814	0.4091	No
(Gb-Antp+Gb-Ubx) VS. Antp A4	X2	2.4911	0.1144	No
(Gb-Antp+Gb-Ubx) VS. Antp A5	FE	N/A	1.0000	No
(Gb-Antp+Gb-Ubx) VS. Ubx A1	FE	N/A	1.0000	No
(Gb-Antp+Gb-Ubx) VS. Ubx A2	X2	22.8716	< .00001	Yes
(Gb-Antp+Gb-Ubx) VS. Ubx A3	X2	3.6863	0.0548	No
(Gb-Antp+Gb-Ubx) VS. Ubx A4	X2	15.5755	0.0000	Yes
(Gb-Antp+Gb-Ubx) VS. Ubx A5	FE	N/A	0.2398	No
(Gb-Ubx+Gb-abd-A) VS. Ubx A1	FE	N/A	1.0000	No
(Gb-Ubx+Gb-abd-A) VS. Ubx A2	X2	0.0355	0.8504	No
(Gb-Ubx+Gb-abd-A) VS. Ubx A3	X2	6.6956	0.0096	Yes
(Gb-Ubx+Gb-abd-A) VS. Ubx A4	X2	8.2739	0.0040	Yes
(Gb-Ubx+Gb-abd-A) VS. Ubx A5	FE	N/A	1.0000	No
(Gb-Ubx+Gb-abd-A) VS. abd-A A1	FE	N/A	0.5338	No
(Gb-Ubx+Gb-abd-A) VS. abd-A A2	X2	0.5093	0.4754	No
(Gb-Ubx+Gb-abd-A) VS. abd-A A3	X2	2.954	0.0856	No
(Gb-Ubx+Gb-abd-A) VS. abd-A A4	X2	6.0295	0.0140	Yes
(Gb-Ubx+Gb-abd-A) VS. abd-A A5	FE	N/A	1.0000	No
(Gb-Antp+Gb-abd-A) VS. Antp A1	FE	N/A	0.2589	No
(Gb-Antp+Gb-abd-A) VS. Antp A2	X2	5.5567	0.0184	Yes
(Gb-Antp+Gb-abd-A) VS. Antp A3	FE	N/A	0.1150	No
(Gb-Antp+Gb-abd-A) VS. Antp A4	X2	2.7686	0.0961	No
(Gb-Antp+Gb-abd-A) VS. Antp A5	FE	N/A	0.0706	No
(Gb-Antp+Gb-abd-A) VS. Antp A6	FE	N/A	0.0000	Yes
(Gb-Antp+Gb-abd-A) VS. abd-A A1	FE	N/A	0.6521	No
(Gb-Antp+Gb-abd-A) VS. abd-A A2	X2	0.0204	0.8865	No
(Gb-Antp+Gb-abd-A) VS. abd-A A3	FE	N/A	0.0013	Yes
(Gb-Antp+Gb-abd-A) VS. abd-A A4	X2	10.395	0.0012	Yes
(Gb-Antp+Gb-abd-A) VS. abd-A A5	FE	N/A	0.0208	Yes
(Gb-Antp+Gb-abd-A) VS. abd-A A6	FE	N/A	0.0000	Yes

Table S8. Primers used for gene cloning and qPCR.

Gene name / primer name	Gene region targeted	length (bp)	Forward primers (5'-3')	Reverse primers (5'-3')
Gb-Scr, qPCR	ORF	91	AAGAAGGAGCACAAGATGGC	AGGGCCGCATTTTTACAGTG
Gb-Antp, qPCR	ORF	136	GCGCATGAAGTGGAAGAAAGAG	GCTATAAATTAGGGGCGTGTGG
Gb-Ubx, qPCR	ORF	117	AGCGATCAAAGAGCTCAACG	AGGAAACTCGACTCTTCTCGAC
Gb-abd-A, qPCR	ORF	121	TTCTCAAGGCAGTGGCAAAG	TGAACGCAGATGAGGCATTG
Gb-eya	ORF	950	AGGGACAGTGCTTGTGAAGG	ACACACGAGTCAATCACTGG
Gb-six4	ORF	321	CTGTACAGCATCCTGGAGGG	GAACCAGTTGCTGACTTGCG